

國立臺灣大學理學院物理學所

碩士論文

Graduate Institute of Physics

College of Science

National Taiwan University

Master Thesis



標準模型之實數純量擴展：

電弱相變之規範與方策依賴探討

Standard Model with a Real Singlet Scalar: An
Investigation of Scheme Dependence and Gauge
Dependence in Electroweak Phase Transition

李彥頌

Yen-Ting Li

指導教授：蔣正偉 博士

Advisor: Cheng-Wei Chiang, Ph.D.

中華民國 107 年 11 月

November, 2018



誌謝

感謝 蔣正偉老師的指導，我很感恩在他碩班所教導的一切，也很幸運有一位學術上要求嚴格但個性上充滿溫暖的指導老師。我十分感激 Senaha Eibun 的仔細且細心的教導，無論是多細微的問題都請囊相授，其受用無窮。感謝口試委員 何小剛 與 吳建宏老師在口試時提供有趣的問題，讓我可以從不同的面向思考。感謝郭安立學姊幫我校正英文上的錯誤，和提供有關未來物理研究上的想法。感謝黃程楷學長與我一起討論 Mathematica 上的問題。感謝林于翔學長提供我如何使用 MicrOMEGAs 計算 relic density。

最後我要感激家人給予經濟上與精神上的支持，也感謝我許多的朋友在一路上的幫助。



Acknowledgements

I would like to express my great appreciation to Prof. Cheng-Wei Chiang for everything he told me in this period. I am fortunate to have a supervisor who is strict in academic and also is empathetic in personality. I would like to offer my deep gratitude to Dr. Eibun Senaha for his patient and dedicated guidance. I learn numerous valuable lessons from him. He devotedly discusses every trivial question with me which I benefited vastly. I would also thank Prof. Xiao-Gang He and Prof. Kin-Wang Ng for providing useful critiques in the oral defence.

I would also like to extend my thanks to my seniors. Thanks Dr. An-Li Kuo for improving my English grammar, and I am also appreciated her for providing useful advise for the future research path. Thanks Mr. Cheng-Kai Huang for discussing and solving the Mathematica problems with me. Thanks Mr. Yu-Xiang Lin for teaching me how to use the MicrOMEGAs for calculating relic density. Many thanks to countless friends for helping me go through the master degree.

Finally, I wish to thank my parents and sister for their long-lasting support and encouragement throughout my study.



摘要

為了實現兩步電弱相變，此碩論探討了將標準模型擴增一個實數單態粒子。我們利用許多不同方策 (scheme) 去探討且量化模型中的方策以及規範依賴。在考慮第一階圈圖計算時，on-shell (OS)-like 方策中的 Nambu-Goldstone 波色子需要被重求和以避免紅外發散，而我們量化其重求和後對電弱相變的影響。在 OS-like 以及 \overline{MS} 方策中，兩者所計算的電弱相變之臨界溫度相當一致。在規範依賴的探討中，採用 High-temperature 以及 Patel-Ramsey-Musolf 方策來做比較。在某些方策中，分析出的結果對重整化能量尺度有依賴性，此顯示了高階修正是必須的。但無論是對規範有依賴或無依賴的方策，最終資料分析顯示，兩者都在理論誤差以內。

關鍵字：有效場論，微擾理論，規範依賴，規範場論，重整化，重求和，電弱作用，臨界現象，數值計算，數值方法



Abstract

In this thesis, the standard model is extended with a real singlet scalar S to achieve a two-step electroweak phase transition (EWPT). The model is investigated with several schemes to quantify the scheme dependence and the gauge dependence issue. In on-shell(OS)-like scheme, at the one-loop order, Nambu-Goldstone boson contributions are needed to be resummed to circumvent the IR divergence; their effects in the EWPT are studied and quantified. The critical temperatures and critical vacuum expectation values of the EWPT in the OS-like and the $\overline{\text{MS}}$ schemes are highly consistent to each other; we also compare the results with two gauge-independent schemes (the high temperature and the Patel-Ramsey-Musolf schemes). Even though higher order corrections are needed for scale-dependent schemes, the general trend of the results are consistent and the analyses show the differences of gauge-dependent and -independent schemes are within theoretical uncertainties.

Keywords: effective potential, perturbation theory, gauge dependence, gauge field theory, renormalization, resummation, electroweak interaction, critical phenomena, numerical calculations, numerical methods



Contents

口試委員審定書

誌謝 ii

Acknowledgements iii

摘要 iv

Abstract v

1 Introduction 1

2 Model: SM + Real Singlet Scalar 8

2.1 On-shell-like Scheme (OS-like) 10

2.2 $\overline{\text{MS}}$ Scheme 12

2.3 Thermal History and Thermal Potential 13

2.3.1 Standard method of searching T_C and critical VEVs 14

2.4 High Temperature (HT) 15

2.5 Patel-Ramsey-Musolf (PRM) Scheme 15

2.5.1 Gauge-independent T_C and VEVs 16

3 Numerical Analysis 18

3.1 Critical Temperature and Critical VEV 19

3.2 (non)Thermal Gauge and NG Boson Contribution 20

3.3 Scheme Dependence Comparison 22

3.4 Scale Dependence of T_C 24

4 Discussion and Conclusion	26
4.1 Discussion: Dark Matter, Vacuum Stability and Perturbativity	26
4.2 Conclusion	27
A Generating Functional of 1(not 1)-PI	28
B Effective Potential in One-Loop	31
C Approximate Thermal Function	36
C.1 Boson	36
C.1.1 HTEB ($a < 0.35$)	37
C.1.2 PFFB ($0.35 \leq a \leq 9.0$)	37
C.1.3 LTEB ($a > 9.0$)	38
C.1.4 Bessel Approximation for $a \in i\mathfrak{R}$	38
C.2 Fermion	39
C.2.1 HTEF ($a < 0.32$)	39
C.2.2 PFFF ($0.32 \leq a \leq 9.0$)	39
C.2.3 LTEF ($a > 9.0$)	40
C.2.4 $a \in i\mathfrak{R}$	40
D Field-Dependent Mass	41
D.1 Higgs Bosons	41
D.2 NG Bosons	42
D.3 Gauge Boson	43
D.4 Top Quark	44
E An Illustrative Application PRM	45
E.1 Gauge-invariant T_C	52
Bibliography	54





List of Figures

- 3.1 The contour plots of the HT effective potential in the plane of $\langle\phi\rangle$ and $\langle\phi_S\rangle$ at $T = 300$ GeV (Upper Left), $T = T_C + 10$ GeV (Upper Right), $T = T_C = 75.1$ GeV (Middle Left), $T = T_C - 10$ GeV (Middle Right) and $T = 0$ GeV (Lower). The parameters are, $m_S = m_H/2$ and $\lambda_{HS} = 0.4$. Note that all the plot legends are in the unit of 10^7 GeV. 21
- 3.2 The effect of thermal (TGB off, red dot-dashed), non-thermal gauge (GB off, green dashed) and NG bosons (NG off, yellow dotted) contributions on T_C (Left panel) and v_C/T_C (Right panel) in the OS-like scheme. The blue solid line includes all the contributions. 22
- 3.3 Comparison of scheme-depended results and investigation of scale dependence. *Left*: Critical temperature as the function of λ_{HS} . *Right*: v_C/T_C as the function of λ_{HS} . The OS-like scheme with NG resummation and the HT scheme are depicted as the blue solid and black dotted lines, respectively. For the $\overline{\text{MS}}$ and the PRM schemes, the style of lines are green and red, respectively. In the legend, “MS2mt (MS05mt)” represents that the $\overline{\text{MS}}$ scheme’s renormalization scale is at $2m_t(m_t/2)$. Same notation is also applied to the PRM scheme. 23
- 3.4 Critical temperature as the function of renomalization scale in the $\overline{\text{MS}}$ scheme. The parameter settings are $\lambda_{HS} = 0.2$ and $m_S = m_H/2$. The spike around 109 GeV is expected to be an accidental cancellation among contributions of different particle contents, not any physical or theoretical interest. 25



List of Tables

3.1	The input parameters in all schemes. Note that, besides the $\overline{\text{MS}}$ scheme (see Sec. 2.2), μ_H , μ_S , and λ_H satisfy the tree-level relations: $\mu_H^2 = m_H^2/2$, $\mu_S^2 = -m_S^2 + \lambda_{HS}/2v_0^2$ and $\lambda_H = m_H^2/2v_0^2$	18
3.2	Summary of the scheme settings.	19
3.3	The percentage of the effects on the EWPT by turning off specific channel.	22



Chapter 1

Introduction

Cosmic baryon asymmetry (BA) problem [1, 2] is a long-standing and ongoing topic in particle physics and cosmology. Electroweak baryogenesis (EWBG), one of the most promising mechanisms to solve BA, requires a strong first-order electroweak phase transition (EWPT) which creates electroweak(EW)-symmetry-breaking bubble. CP-violating interactions occur at the bubble wall and induce a net density of left-handed fermions. This process makes EW sphalerons produce unequal amounts of baryons and anti-baryons. For a successful EWBG theory, the baryon-number-changing processes have to sufficiently suppress inside the expanding EW-breaking bubbles in order to prevent the wash out. The criterion for above is*

$$\frac{\text{critical vacuum expectation value, } v_c}{\text{critical temperature, } T_C} > \zeta_{\text{sph}}(T_C), \quad (1.1)$$

where $\zeta_{\text{sph}}(T_C)$ depends on the sphaleron configuration (or topology) [3] and the fluctuation determinant [4], *etc.* The current model [5] has showed that $\zeta_{\text{sph}}(T_C) \simeq 1.1 - 1.2$, where the one-loop effective potential with thermal resummation is used to evaluate the sphaleron energy. However, EWBG cannot be achieved by the standard model (SM) alone, since the discovered Higgs boson with 125 GeV [6] is incompatible to the mechanism required. To be more specifically, in the SM, the first-order EWPT cannot take

*The critical phenomenology occurs when the potential energy of minima are degenerated and the tunnelling process happens, *i.e.*, the first-order phase transition from EW-symmetry vacuum to EW-breaking vacuum takes place.

place; instead, the EWPT is a smooth crossover [7]. Further, baryon number will be erased due to the sphaleron processes. By extending the scalar sector with an $SU(2)_L$ singlet scalar (S), this simplest extension can provide a viable parameter space that makes the first-order EWPT possible. Furthermore, S can also be a dark matter (DM) candidate by imposing a Z_2 symmetry [8, 9].

In principle, every physical observable should be independent of any artificial effect. For example, the full Higgs potential should be a gauge-independent quantity. Nevertheless, in practice, one has to truncate the calculation at a certain level since the full exact analytical form of potential cannot be obtained (in other words, full-loop calculation cannot be achieved). Perturbative effective potential is widely used to analyse EWPT; especially, one- or two-loop expansions are often adopted for various analyses. However, it is well known that any result from this method is depended on the gauge fixing parameter (ξ) [10]. For instance, the Higgs vacuum expectation value (VEV) is varying as one changes ξ . Furthermore, this gauge-dependent issue will contaminate the calculation of baryon-number preservation criterion, Eq. (1.1). As a result, any phenomenological claim and consequence is inherited this ξ dependence. Therefore, the gauge effect should be regularized. To be note that one of the exceptions is when the EWPT is driven by the scalar thermal loops or the tree-level barrier where the ξ dependence can be neglected. However, in the singlet extended Abelian-Higgs model, as [11] found that the ξ dependence cannot be ignore even when the presence of the tree-level barrier. This issue is seldom investigated deeply in the context of studying EWPT by SM plus real singlet model.

Apart from the artificial gauge problem, another issue in the effective potential calculations is the occurrence of infrared (IR) divergences. The Higgs mass is obtained from the second derivative of the effective potential. If one adopts a renormalization scheme that one-loop level potentials do not affect the tree-level mass relation, the second derivatives of the Nambu-Goldstone (NG) bosons one-loop potential are ill-defined when ξ in the R_ξ gauge is set as zero. Thus, the Higgs mass is IR divergent in this case. One prescription to resolve is to include higher order terms into the NG boson masses [12, 13], *i.e.*, resumming the NG boson masses. In the later, we will show that after the NG masses are resummed,

their contributions to the Higgs mass are relatively minor compared with other effects. Nevertheless, their numerical effects on v_C/T_C are unexplored.

In this thesis, the EWPT is revisited in the context of the SM with a real singlet scalar. To unfold the gauge problem aforementioned, we first analyse the degree of effect on v_C/T_C by subtracting both thermal and non-thermal gauge boson contributions from the effective potential. Even though the exact ξ dependence in the potential cannot be shown in this simple analysis, one can demonstrate numerically the importance of gauge channels in the successful first-order EWPT ($v_C/T_C \geq 1$), as the ξ dependence mainly comes from the gauge contributions. This method stands as a criterion for whether the investigation of ξ dependence is necessary. Meanwhile, the numerical impact on the NG resummation in the on-shell(OS)-like scheme[†] is also analysed.

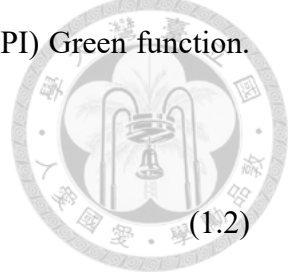
To avoid the scheme dependence issue, three commonly adopted schemes in the literature are also investigated: (1) the $\overline{\text{MS}}$ scheme, (2) the high-temperature (HT) scheme and (3) the Patel-Ramsey-Musolf (PRM) scheme [4]. In the first scheme, unlike the OS-like scheme, the tree-level NG boson masses are non-zero, since the tree-level relations have been modified because of different tadpole conditions; thus, the aforementioned NG resummations are not required. The potential of the second scheme is defined as: the tree-level potential plus the scalar thermal mass terms only. Obviously, the potential is gauge-independent, because the thermal masses are free of the ξ dependence. In the last scheme, the Nielsen-Fukuda-Kugo (NFK) identity [15, 16] is adopted to obtain the gauge-invariant T_C ; v_C is evaluated at the HT potential at T_C in order to keep gauge-invariant. In the last scheme, taking different potentials to obtain T_C and v_C may seem inconsistent. However, this treatment grants the results are strictly gauge-invariant. Note that the numerical comparison between the PRM scheme and the other gauge-dependent schemes has not performed yet, this is one of our goals to complement this work.

The effective potential is the major ingredient of analyzing EWPT and spontaneous symmetry breaking. For completeness, we briefly introduce the derivation of the effective potential from the partition functional (see [17]) by using the Feynman path integral

[†]In [14], this scheme is called the on-shell scheme. Because this is not the genuine on-shell renormalization, we call this scheme the on-shell-like scheme instead.

method [18]. The effective potential in a more specific terminology should be called the generating functional for zero-momentum one-particle irreducible (1PI) Green function. To begin with, we first recall $W[J]$,

$$\mathcal{Z}[J] = e^{iW[J]} \quad (1.2)$$



which is the generating functional for connected Green's functions (the detail of generating functional of connecting Green function is shown in Appendix A). Expressing the partition functional, $\mathcal{Z}[J]$, with an external source field, $J(x)$, in the path integral representation, we have

$$\mathcal{Z}[J] = N \int D\phi e^{i \int d^4x [\mathcal{L}(\phi) + J(x)\phi(x)]} = \langle 0^+ | 0^- \rangle, \quad (1.3)$$

$$\text{where } N^{-1} = \int D\phi e^{i \int d^4x [\mathcal{L}(\phi)]}. \quad (1.4)$$

The second equality of Eq. (1.3) is a reminder that the partition function represents a state starts with a no particle state at $+\infty$ position and end with a no particle state at $-\infty$ position. The VEV of ϕ in the presence of J can be defined by

$$\begin{aligned} \phi_c(y) &= \frac{\delta W[J]}{\delta J(y)} = \frac{\int D\phi \phi(y) \exp(i \int d^4x [\mathcal{L}(\phi) + J(x)\phi(x)])}{\int D\phi \exp(i \int d^4x [\mathcal{L}(\phi) + J(x)\phi(x)])}, \\ &= \langle 0^+ | \phi(y) | 0^- \rangle_J, \end{aligned} \quad (1.5)$$

the last equality shows that ϕ_c is actually a classical field. The physical VEV is

$$\varphi(y) = \left. \frac{\delta W[J]}{\delta J(y)} \right|_{J=0} = N \int D\phi \phi(y) e^{i \int d^4x [\mathcal{L}(\phi)]} = \langle 0^+ | \phi(y) | 0^- \rangle. \quad (1.6)$$

Furthermore, if we assume that the vacuum has a translational symmetry, the VEV does not depend on the spacetime position any more, *i.e.*,

$$\phi = \langle 0 | \phi(x) | 0 \rangle = \langle 0 | e^{iPx_1} \phi(0) e^{-iPx_2} | 0 \rangle = \langle 0 | \phi(0) | 0 \rangle = \text{constant field}. \quad (1.7)$$

Motivated by the idea that finding a generating functional provides 1PI connect Green

function, the effective action provides the exact role. The effective action is defined as a Legendre transformation of $W[J]$,

$$\begin{aligned}
 \Gamma[\phi_c] &= W[J] - \int d^4x \phi_c(x) J(x), \\
 &= -i \left\{ \ln N \int D\phi \exp \left[i \int d^4x (\mathcal{L}(\phi) + J(x)\phi(x)) \right] \right\} \\
 &\quad - i \left\{ \ln \exp \left[(-i) \int d^4x J(x)\phi_c(x) \right] \right\}, \\
 &= -i \left\{ \ln N \int D\phi \exp \left[i \int d^4x (\mathcal{L}(\phi) + J(x) (\phi(x) - \phi_c(x))) \right] \right\}.
 \end{aligned} \tag{1.8}$$



In addition,

$$\frac{\delta \Gamma[\phi_c]}{\delta \phi_c(x)} = J[x], \tag{1.9}$$

which can be proved straight forward. The advantage of effective function can be understood from the following: while the source field is turning off, ϕ_c that satisfies Eq. (1.9) is the lowest energy configuration of the theory. This solution has particularly interest in the spontaneous symmetry breaking analysis. The same idea is also applied to the effective potential which will be demonstrated in the later. By shifting the field, $\phi' = \phi - \phi_c$ (the position index is omitted hereafter), and using the definition of action: $S(\phi) = \int d^4x \mathcal{L}(\phi)$, Eq. (1.8) becomes

$$\Gamma[\phi_c] = -i \ln N \int D\phi' \exp \left\{ i \left[S(\phi_c + \phi') + \int d^4x J\phi' \right] \right\}. \tag{1.10}$$

The small shifting of the field can be approximated by expanding the action around the classical field (ϕ_c),

$$\begin{aligned}
 S[\phi_c + \phi'] &= S[\phi_c] + \int d^4x \frac{\delta S[\phi_c + \phi']}{\delta \phi} \Big|_{\phi'=0} \phi' \\
 &\quad + \frac{1}{2} \int d^4x d^4y \phi'(x) \frac{\delta^2 S[\phi_c + \phi']}{\delta \phi(x) \delta \phi(y)} \Big|_{\phi'=0} \phi'(y) + \dots.
 \end{aligned} \tag{1.11}$$

The action satisfies the variational principle; hence

$$\begin{aligned} \left. \frac{\delta S[\phi_c + \phi']}{\delta \phi} \right|_{\phi'=0} &= \frac{\delta S[\phi_c]}{\delta \phi_c} = 0, & \left. \frac{\delta^2 S[\phi_c + \phi']}{\delta \phi(x) \delta \phi(y)} \right|_{\phi'=0} &= \frac{\delta^2 S[\phi_c]}{\delta \phi_c(x) \delta \phi_c(y)}, \\ & & &= iG^{-1}(x, y; \phi_c), \end{aligned} \quad (1.12)$$

where G is the two-point Green function. Then Eq. (1.11) can be arranged into

$$S[\phi_c + \phi'] = S[\phi_c] + 0 + \frac{1}{2} \int d^4x d^4y \phi(x) iG^{-1}(x, y; \phi_c) \phi(y) + \dots \quad (1.13)$$

Because $S[\phi_c]$ is independent of ϕ , one can bring it out of the integral; then the effective action becomes

$$\Gamma[\phi_c] = S[\phi_c] - i \ln N \int D\phi' \exp \left\{ \frac{1}{2} \int d^4x d^4y \phi(x) G^{-1}(x, y; \phi_c) \phi(y) \right\} + \dots \quad (1.14)$$

The second term can be evaluated by utilizing the equality,

$$\int_{-\infty}^{\infty} d\vec{p} e^{-\frac{1}{2} \vec{p}^\dagger \mathbf{A} \vec{p} + \vec{I}^\dagger \vec{p}} = \sqrt{\frac{(2\pi)^n}{\det \mathbf{A}}} e^{\frac{1}{2} \vec{I}^\dagger \mathbf{A} \vec{I}}, \quad (1.15)$$

where n is the d.o.f. of p . In our case, $\vec{I} = 0$ and $\mathbf{A} = iG^{-1}$. After absorbing $\sqrt{(2\pi)^n}$ and N into $D\phi'$, the effective action is

$$\Gamma[\phi_c] = S[\phi_c] + \frac{i}{2} \ln \text{Det} iG^{-1}(x, y; \phi_c) + \dots, \quad (1.16)$$

$$= S[\phi_c] + \frac{i}{2} \hat{\text{Tr}} \ln iG^{-1}(x, y; \phi_c) + \dots, \quad (1.17)$$

$$= S[\phi_c] + \frac{i}{2} \text{Tr} \ln \int d^4x d^4y \delta(x - y) iG^{-1}(x, y; \phi_c) + \dots, \quad (1.18)$$

where the operator Det acts on the spacetime, (x, y) and also any internal space, *e.g.*, color space or spinor space, *etc.* An identity is used: $\text{Det} \mathbf{A} = \exp(\hat{\text{Tr}} \ln \mathbf{A})$, where $\hat{\text{Tr}}$ acts on the same space(s) as Det . Additionally, if the operator \mathbf{A} is a function of spacetime, the functional trace has the property: $\text{Tr} \mathbf{A} = \int d^4x \mathbf{A}(x, x)$ which is adopted in Eq. (1.18). We can simplify the above further by performing the integral and expressing the Green

function in the momentum space, which is convenient for the later use,

$$\Gamma[\phi_c] = S[\phi_c] + \frac{i}{2} \text{Trln} \int d^4x iG^{-1}(x, x; \phi_c) + \dots, \quad (1.19)$$

$$= \int d^4x \mathcal{L}(\phi_c) + \frac{i}{2} \int \frac{d^4p}{(2\pi)^4} \text{Trln} iG^{-1}(p; \phi_c) \int d^4x + \dots, \quad (1.20)$$

$$= -V_0(\phi_c) \int d^4x + \frac{i}{2} \int \frac{d^4p}{(2\pi)^4} \text{Trln} iG^{-1}(p; \phi_c) \int d^4x + \dots, \quad (1.21)$$

where we have assumed that ϕ_c is a constant field, so that kinetic term is absent. Since the tree-level potential is independent of spacetime, it can be brought out of the integral. Finally, the effective potential is defined as the following:

$$\Gamma[\phi_c] \equiv -V_{\text{eff}}(\phi_c) \int d^4x, \quad (1.22)$$

$$V_{\text{eff}}(\phi_c) = V_0(\phi_c) - \frac{i}{2} \int \frac{d^4p}{(2\pi)^4} \text{Trln} iG^{-1}(p; \phi_c) + \dots, \quad (1.23)$$

$$V_1(\phi_c) = -\frac{i}{2} \int \frac{d^4p}{(2\pi)^4} \text{Trln} iG^{-1}(p; \phi_c), \quad (1.24)$$

where V_1 stands for the general one-loop potential of different particle contents. We can now easily understand what the name of effective potential represents: besides the dominant tree-level potential, the effective potential represents the potential that includes all the higher order corrections. In our analysis, we require the level of correction is $\mathcal{O}(\hbar)$ which corresponds to the one-loop level. The detail of derivation of the one-loop level potential for each particle species can be seen in the Appendix B.

The thesis is organized as the following: In Chap. 2, we introduce our model, renormalization schemes and tadpole conditions in each scheme. In addition, the pattern of the EWPT and the method of searching T_C and v_C is outlined. Chap. 3 demonstrates our numerical analyses and we discuss the renormalization-scale dependence on T_C . In the end, we discuss the DM issue in the Sec. 4.1; our results are summarized in the Sec. 4.2.



Chapter 2

Model: SM + Real Singlet Scalar

We consider a model in which $SU(2)_L$ real singlet scalar S is added to the SM. S can be the dark matter candidate by imposing the Z_2 symmetry on the Lagrangian [9] (*i.e.*, it is invariant under $S \rightarrow -S$). We require S can only couple to the Higgs sector (the higgs portal). The tree-level Higgs potential of the theory is the following:

$$V_0(H, S) = -\mu_H^2 H^\dagger H + \lambda_H (H^\dagger H)^4 - \frac{\mu_S^2}{2} S^2 + \frac{\lambda_S}{4} S^4 + \frac{\lambda_{HS}}{2} H^\dagger H S^2, \quad (2.1)$$

where H is the usual complex Higgs doublet. It is written in terms of the components as

$$H(x) = \begin{pmatrix} G^+(x) \\ \frac{1}{\sqrt{2}} [\phi + h(x) + iG^0(x)] \end{pmatrix}, \quad (2.2)$$

where ϕ which will eventually develop the non-zero VEV at $\simeq 246$ GeV represents the constant background field (translational symmetry) of H . The real part of the neutral component of H is $h(x)$, the 125 GeV Higgs boson. $G^{0,\pm}(x)$ stand for the NG bosons. The superscripts refer to the electric charge of the fields. Presenting the potential in terms

of components, we have

$$\begin{aligned}
V_0 = & \frac{-\mu_H^2}{2} \{(\phi + h)^2 + [2G^+G^- + (G^0)^2]\} \\
& + \frac{\lambda_H}{4} \left\{ (\phi + h)^4 + 2(\phi + h)^2 [2G^-G^+ + (G^0)^2] + [2G^-G^+ + (G^0)^2]^2 \right\} \\
& - \frac{\mu_H^2}{2} S^2 + \frac{\lambda_S}{4} S^4 + \frac{\lambda_{HS}}{2} S^2 \{(\phi + h)^2 + [2G^+G^- + (G^0)^2]\}.
\end{aligned} \tag{2.3}$$



The tree-level effective potential can also be represented by using only the constant background fields (denoting background field of S as ϕ_S), by turning off quantum fields (h and $G^{0,\pm}$),

$$V_0(\phi, \phi_S) = -\frac{\mu_H^2}{2}\phi^2 + \frac{\lambda_H}{4}\phi^4 - \frac{\mu_S^2}{2}\phi_S^2 + \frac{\lambda_S}{4}\phi_S^4 + \frac{\lambda_{HS}}{4}\phi^2\phi_S^2. \tag{2.4}$$

In order to bound the potential from below, λ_H and λ_S must be greater than zero. In addition, another condition is necessary if $\lambda_{HS} < 0$. In the region that both ϕ and ϕ_S are large, we can denote $\phi_S = \phi\delta$, where δ is a number. The relevant terms in the potential become

$$V_0 \sim \frac{1}{4}(\lambda_H + \lambda_S\delta^4 + \lambda_{HS}\delta^2)\phi^4. \tag{2.5}$$

To keep the bracket always greater than zero for arbitrary δ , we require

$$\lambda_{HS}^2 < 4\lambda_H\lambda_S, \quad \text{if } \lambda_{HS} < 0. \tag{2.6}$$

Note that a local minimum in the S direction will appear as $\mu_S^2 > 0$. The EW-broken vacuum should be the global minimum in the present universe: $V_0(v, 0) < V_0(0, v_S^{\text{sym}})$, where the superscript means that the singlets VEV is in a EW-symmetry phase. This condition requires that

$$\frac{-\mu_H^2}{2}v^2 + \frac{\lambda_H}{4}v^4 < \frac{-\mu_S^2}{2}(v_S^{\text{sym}})^2 + \frac{\lambda_S}{4}(v_S^{\text{sym}})^4. \tag{2.7}$$

By the minimum conditions at the tree level, $v_S^{\text{sym}} = \sqrt{\mu_S^2/\lambda_S}$ and $\mu_H^2 = \lambda_H v^2$, we can

rearrange above into

$$\lambda_S > \lambda_H \frac{\mu_S^4}{\mu_H^4} \equiv \lambda_S^{\min}. \quad (2.8)$$

In the numerical analyses, we took $\lambda_S = \lambda_S^{\min} + 0.1$. This choice makes first-order phase transition possible and it is also adopted in [14]. Tadpole conditions are scheme-dependent. The general form is

$$T_{h(S)} \equiv \left\langle \frac{\partial V_{\text{eff}}}{\partial \phi_{(S)}} \right\rangle = 0, \quad (2.9)$$

where $\langle \dots \rangle$ denotes that the term inside the bracket is evaluated in a vacuum and all quantum fields are taken as zero. The order of level of the effective potential (tree or loop, *etc.*) is evaluated depends on the corresponding scheme. The Landau gauge ($\xi = 0$) is taken when evaluating the gauge contributions, except the PRM scheme.

2.1 On-shell-like Scheme (OS-like)

The OS-like scheme requires that the loop corrections hold the tree-level relations when the one-loop corrections are added. Therefore, the renormalization conditions are*

$$\left\langle \frac{\partial(V_{\text{CW}} + V_{\text{CT}})}{\partial \phi} \right\rangle = 0, \quad \left\langle \frac{\partial^2(V_{\text{CW}} + V_{\text{CT}})}{\partial \phi^2} \right\rangle = 0, \quad \left\langle \frac{\partial^2(V_{\text{CW}} + V_{\text{CT}})}{\partial \phi_S^2} \right\rangle = 0, \quad (2.10)$$

where V_{CT} are the counter terms, and V_{CW} is the Coleman-Weinberg potential [19]:

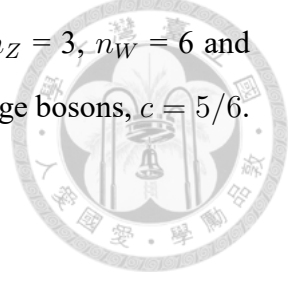
$$V_{\text{CT}} = -\frac{\delta\mu_H^2}{2}\phi^2 - \frac{\delta\mu_S^2}{2}\phi_S^2, \quad (2.11)$$

$$V_{\text{CW}}(\overline{m}_i^2) = \sum_i n_i \frac{\overline{m}_i^4}{4(16\pi^2)} \left(\log \frac{\overline{m}_i^2}{\mu^2} - c_i \right), \quad (2.12)$$

which is regularized in the $\overline{\text{MS}}$ scheme (see Appendix B). \overline{m}_i represents different background-field-dependent masses (see the Appendix D for detail); its subscript stands for a particle's species. We include the Higgs bosons ($H_{1,2}$, eigenstates of the scalar sector), NG bosons

*Note that checking the first derivative of the one-loop potential with respect ϕ_S is trivial, since the Z_2 symmetry guarantees it is zero.

(G^\pm, G^0) , the gauge bosons (W, Z) and top quark (t). The degree of freedom (d.o.f.) and its statistic of the particle is denoted as n_i : $n_{H_{1,2}, G^0} = 1$, $n_{G^\pm} = 2$, $n_Z = 3$, $n_W = 6$ and $n_t = -12$. For the scalars and the top quark, $c = 3/2$, and for the gauge bosons, $c = 5/6$. $\bar{\mu}$ represents the renormalization scale.



The tadpole conditions for the OS-like scheme at the tree level are

$$T_h \equiv \left\langle \frac{\partial V_0}{\partial \phi} \right\rangle = v \left(-\mu_H^2 + \lambda_H v^2 + \frac{\lambda_{HS}}{2} v_S^2 \right) = 0, \quad (2.13)$$

$$T_S \equiv \left\langle \frac{\partial V_0}{\partial \phi_S} \right\rangle = v_S \left(-\mu_S^2 + \lambda_S v_S^2 + \frac{\lambda_{HS}}{2} v^2 \right) = 0, \quad (2.14)$$

where v and v_S are the VEVs of the doublet Higgs and S , respectively. For the Z_2 -invariant EW-broken vacuum ($\phi = v_0, \phi_S = 0$), $\mu_H^2 = \lambda_H v_0^2$ and $v_S^{\text{Br}} = 0$. Therefore, the Higgs boson masses in the vacuum are

$$m_H^2 = \left\langle \frac{\partial^2 V_0}{\partial \phi^2} \right\rangle = -\mu_H^2 + 3\lambda_H v_0^2, \quad (2.15)$$

$$m_S^2 = \left\langle \frac{\partial^2 V_0}{\partial \phi_S^2} \right\rangle = -\mu_S^2 + \frac{\lambda_{HS}}{2} v_0^2. \quad (2.16)$$

NG Resummation

If we use Eq. (2.12) to evaluate the second condition of Eq. (2.10), one can notice that while m_i equals to zero, which is the case for the NG bosons at the electroweak vacuum, a IR divergent term appears: $\lambda_H^2 \phi^2 (\log \bar{m}_G^2 / \bar{\mu}^2) |_{\phi \rightarrow v_0}$; regardless of what the value of $\bar{\mu}$ is. However, the existence of a IR problem often indicates that a theory is incomplete. In this case, it shows that the necessity of including the higher order correction to the NG boson masses, *i.e.*, we need to resum the NG boson contributions. We adapt the same procedure as [12, 13], $\bar{m}_G \rightarrow \bar{M}_G = \bar{m}_G + \bar{\Sigma}_G$, where $\bar{\Sigma}_G$ is the one-loop self-energy of the NG

boson with the vanishing external momenta:

$$\begin{aligned} \bar{\Sigma}_G = \frac{1}{16\pi^2} & \left[3\lambda_H \bar{m}_{H_1}^2 \left(\log \frac{\bar{m}_{H_1}^2}{\bar{\mu}^2} - 1 \right) + \frac{1}{2} \lambda_{HS} \bar{m}_{H_2}^2 \left(\log \frac{\bar{m}_{H_2}^2}{\bar{\mu}^2} - 1 \right) \right. \\ & + \frac{3g_2^2}{2} \bar{m}_W^2 \left(\log \frac{\bar{m}_W^2}{\bar{\mu}^2} - \frac{1}{3} \right) + \frac{3(g_2^2 + g_1^2)}{4} \bar{m}_Z^2 \left(\log \frac{\bar{m}_Z^2}{\bar{\mu}^2} - \frac{1}{3} \right) \\ & \left. - 6y_t^2 \bar{m}_t^2 \left(\log \frac{\bar{m}_t^2}{\bar{\mu}^2} - 1 \right) \right], \end{aligned} \quad (2.17)$$

where g_1 and g_2 are the gauge couplings of U(1) and SU(2)_L, respectively, and y_t is the top Yukawa coupling. To solve $\delta\mu_H^2$, $\delta\mu_S^2$ and $\bar{\mu}$ numerically, we need to $\bar{m}_G \rightarrow \bar{M}_G$ in the NG boson channels of Eq. (2.12), and combine the CT terms (Eq. 2.11); finally, solve the renormlization conditions Eq (2.10), simultaneously.

2.2 $\overline{\text{MS}}$ Scheme

In the $\overline{\text{MS}}$ scheme, the tree-level relations are modified when the higher-order corrections are added in. In the other words, Eq. (2.15) and Eq. (2.16) will be modified by one-loop level contributions. We impose the tadpole conditions on the one-loop level,

$$T_h \equiv \left\langle \frac{\partial(V_0 + V_1)}{\partial\phi} \right\rangle = v \left(-\mu_H^2 + \lambda_H v^2 + \frac{\lambda_{HS}}{2} v_S^2 \right) + \left\langle \frac{\partial V_{\text{CW}}}{\partial\phi} \right\rangle = 0, \quad (2.18)$$

$$T_S \equiv \left\langle \frac{\partial(V_0 + V_1)}{\partial\phi_S} \right\rangle = v_S \left(-\mu_S^2 + \lambda_S v_S^2 + \frac{\lambda_{HS}}{2} v^2 \right) + \left\langle \frac{\partial V_{\text{CW}}}{\partial\phi_S} \right\rangle = 0, \quad (2.19)$$

by using the same solution like above ($\phi = v_0, \phi_S = 0$); as a result, we have relations

$$\mu_H^2 = \lambda_H v_0^2 + \frac{1}{v_0} \left\langle \frac{\partial V_{\text{CW}}}{\partial\phi} \right\rangle, \quad (2.20)$$

$$\left\langle \frac{\partial V_{\text{CW}}}{\partial\phi_S} \right\rangle = 0. \quad (2.21)$$

The Higgs masses are

$$m_H^2 = \left\langle \frac{\partial^2(V_0 + V_1)}{\partial\phi^2} \right\rangle = \left(-\mu_H^2 + 3\lambda_H v^2 + \frac{\lambda_{HS}}{2} v_S^2 \right) + \left\langle \frac{\partial^2 V_{CW}}{\partial\phi^2} \right\rangle, \quad (2.22)$$

$$m_S^2 = \left\langle \frac{\partial^2(V_0 + V_1)}{\partial\phi_S^2} \right\rangle = \left(-\mu_S^2 + 3\lambda_S v_S^2 + \frac{\lambda_{HS}}{2} v^2 \right) + \left\langle \frac{\partial^2 V_{CW}}{\partial\phi_S^2} \right\rangle. \quad (2.23)$$

Rearranging above by inputting the solution ($\phi = v_0, \phi_S = 0$) and using Eq. (2.20), we have

$$m_H^2 = 2\lambda_H v_0^2 - \frac{1}{v_0} \left\langle \frac{\partial V_{CW}}{\partial\phi} \right\rangle + \left\langle \frac{\partial^2 V_{CW}}{\partial\phi^2} \right\rangle, \quad (2.24)$$

$$m_S^2 = -\mu_S^2 + \frac{\lambda_{HS}}{2} v_0^2 + \left\langle \frac{\partial^2 V_{CW}}{\partial\phi_S^2} \right\rangle. \quad (2.25)$$

We can solve μ_S, μ_H and λ_H through Eq. (2.24), Eq. (2.25) and Eq. (2.18), numerically.[†] Note that we set the renormalization scale of Eq. (2.12) at the range from $2m_t \sim 0.5m_t$. Since the NG boson masses are non-zero at the electroweak-broken vacuum, we do not need resummation as the OS-like scheme.

2.3 Thermal History and Thermal Potential


Like [20] pointed out that a two-step phase transition pattern increases the accessibility of EWBG. The pattern of two-step phase transition we are interested in is the following: the global vacuum of the early hot universe was $(\phi, \phi_S) = (0, 0)$. While the universe was cooling down, a primary phase transition (PT) occurred, the global minimum are transited to singlet direction (S) at $(0, v_{SC})$, an EW-symmetry-preserving minimum. As the universe approached a critical temperature (T_C) where the potential energy of doublet (H) and singlet minima are degenerate, the global vacuum tunnelled (required to be a first-order PT) to an EW symmetry-breaking minimum $(v_C, 0)$. At the present universe whose temperature is approximately zero, the vacuum arrived at $(v_0 \simeq 246 \text{ GeV}, 0)$.

To investigate above scenario, the dynamic of thermal potential is essential for study-

[†]In Eq. (2.24), actually, the basis of the scalar sector for calculating V_{CW} does not limit to the mass eigenstates; h, S basis is also available, due to the absence of hhS coupling. On the other hand, in Eq. (2.25), one must use mass eigenstates because of the existence SSh coupling.

ing the evolution of the universe. In the OS-like, the $\overline{\text{MS}}$ and the PRM (Sec. 2.5) schemes, we use the finite-temperature one-loop effective potential given by [21]:

$$V_1^T(\phi, \phi_S, T) = \sum_i n_i \frac{T^4}{2\pi^2} I_{B,F} \left(\frac{\overline{m}_i^2}{T^2} \right),$$

$$\text{where } I_{B,F}(a^2) = \int_0^\infty dx x^2 \ln \left(1 \mp e^{-\sqrt{x^2+a^2}} \right).$$
(2.26)


In the numerical computation, we use the approximated functions (see Appendix C) for computational efficiency. In addition, since the perturbative expansion is invalid when temperature is high, the thermal potential needs to be resummed. We replace \overline{m}_i^2 with thermally corrected masses,

$$\overline{m}_i^2 \longrightarrow \overline{m}_i^2 + \Sigma_i(\phi, \phi_S, T),$$
(2.27)

where $\Sigma_i(\phi, \phi_S, T)$ are the thermal masses (a more refined resummation method can be referred to, *e.g.*, [22]), the exact forms can be found in the Appendix D. Notice that although thermal resummation is performed in the OS-like and the $\overline{\text{MS}}$ schemes, it is not performed in the PRM scheme; since we consider only $\mathcal{O}(\hbar) = 1$ in the PRM scheme (see Sec. 2.5 for detail) and the thermal resummation is $\mathcal{O}(\hbar) = 2$ effect.

2.3.1 Standard method of searching T_C and critical VEVs

For a successful two-step EWPT, v_C , T_C , v_{SC}^{Br} and v_{SC}^{sym} are found numerically through the following equations and satisfying the inequalities:

$$V_{\text{eff}}(\phi = v_C, \phi_S = v_{SC}^{\text{Br}}, T_C) = V_{\text{eff}}(\phi = 0, \phi_S = v_{SC}^{\text{sym}}, T_C),$$
(2.28)

$$\left. \frac{\partial V_{\text{eff}}}{\partial \phi} \right|_{v_C, v_{SC}^{\text{Br}}, T_C} = \left. \frac{\partial V_{\text{eff}}}{\partial \phi_S} \right|_{0, v_{SC}^{\text{sym}}, T_C} = 0,$$
(2.29)

$$\left. \frac{\partial^2 V_{\text{eff}}}{\partial \phi_{(S)}^2} \right|_{v_C, v_{SC}^{\text{Br}}, T_C} (0, v_{SC}^{\text{sym}}, T_C) > 0,$$
(2.30)

$$\det \begin{vmatrix} \partial^2 V_{\text{eff}}/\partial\phi^2 & \partial^2 V_{\text{eff}}/\partial\phi\partial\phi_S \\ \partial^2 V_{\text{eff}}/\partial\phi_S\partial\phi & \partial^2 V_{\text{eff}}/\partial\phi_S^2 \end{vmatrix}_{v_C, v_{SC}^{\text{Br}}, T_C (0, v_{SC}^{\text{sym}}, T_C)} > 0, \quad (2.31)$$

where the last two inequalities assure that the minima are not saddle points. In Sec.2.5, we will discuss that why the standard method of determining T_C and VEVs depends on the choice of gauge.

2.4 High Temperature (HT)

Both the OS-like and the $\overline{\text{MS}}$ schemes have gauge-dependent potential at the one-loop level. The high temperature approximation scheme provides a gauge-free and efficient method to investigate EWPT. This scheme simply includes the tree-level potential and the Higgs thermal mass terms which are taken from high temperature approximation at the $\mathcal{O}(2)$ of Eq. (C.1.1):

$$V^{\text{HT}}(\phi, \phi_S, T) = V_0(\phi, \phi_S) + \frac{1}{2}\Sigma_H(T)\phi^2 + \frac{1}{2}\Sigma_S(T)\phi_S^2, \quad (2.32)$$

where Σ_H and Σ_S are the Higgs thermal masses which are gauge-independent [23], see Eq. (D.5, D.6) for detail. Because this scheme is gauge-free and ignores all the other loop contributions, we can obtain the gauge-invariant T_C and VEVs from this potential in relatively efficient way compared with previous schemes. In the PRM scheme (Sec. 2.5), we also use this potential to evaluate VEVs.

2.5 Patel-Ramsey-Musolf (PRM) Scheme

The main goal of the PRM scheme is to get gauge-free results. Unlike the HT scheme, the PRM scheme takes the one-loop order corrections and the thermal effects into account. As the tadpole conditions are set at the tree level, the tree-level conditions are preserved. The renormalization scale is set same as the $\overline{\text{MS}}$ scheme which is varied from $2m_t \sim 0.5m_t$. In the next subsection, we elaborate how the PRM scheme utilizes NFK identity to get gauge-free results.

2.5.1 Gauge-independent T_C and VEVs

The NFK identity [15, 16] tells us that[‡]

$$\frac{\partial V_{\text{eff}}(\phi, \xi)}{\partial \xi} = -C(\phi, \xi) \frac{\partial V_{\text{eff}}(\phi, \xi)}{\partial \phi}, \quad (2.33)$$

where $C(\phi, \xi)$ is a functional. In fact, T_C can be proved formally to be gauge-independent with the identity and Eq. (2.28)[4] as long as we are working on the *full* order of the effective potential. However, in the practical calculation for T_C , one could only calculate the potential up to some order. For example, like in our previous standard method of determining T_C includes only the one-loop order effect; thus, this causes an artificial violation of the NFK identify, even though the full order formalism is gauge-invariant. In order to regulate this issue, we have to keep tracking whether the identity is valid in each order of \hbar . In the perturbation theory, in principle, we can expand V_{eff} and C in the power of \hbar :

$$V_{\text{eff}}(\phi) = V_0(\phi) + \hbar V_1(\phi, \xi) + \hbar^2 V_2(\phi, \xi) + \dots, \quad (2.34)$$

$$C(\phi, \xi) = c_0 + \hbar c_1(\phi, \xi) + \hbar^2 c_2(\phi, \xi) + \dots. \quad (2.35)$$

By inserting them into Eq. (2.33), we get

$$\begin{aligned} \hbar \frac{\partial V_1(\phi, \xi)}{\partial \xi} + \hbar^2 \frac{\partial^2 V_2(\phi, \xi)}{\partial \xi^2} + \dots = & -c_0 \frac{\partial V_0}{\partial \phi} - \hbar \left(c_1(\phi, \xi) \frac{\partial V_0(\phi)}{\partial \phi} \right. \\ & \left. + c_0 \frac{\partial V_1(\phi, \xi)}{\partial \phi} \right) + \mathcal{O}(\hbar^2) + \dots, \end{aligned} \quad (2.36)$$

where we had expressed Eq. (2.33) in \hbar order. Since the tree-level potential is free of ξ -dependence, $c_0 = 0$. At $\mathcal{O}(\hbar)$,

$$\frac{\partial V_1(\phi, \xi)}{\partial \xi} = c_1(\phi, \xi) \frac{\partial V_0(\phi)}{\partial \phi}. \quad (2.37)$$

[‡]Even though our potential is a two dimensional (ϕ, ϕ_S) function, the procedure is straight forward: by taking the other dimensions as zero, one can get a pair of Eq. (2.33). Using the same method described in above, one can get similar results.



Eq. (2.37) shows that as long as we are working on $\mathcal{O}(\hbar)$, the gauge dependence of $V_1(\phi, \xi)$ is vanished at stationary point(s) of the tree-level potential. On the contrary, T_C and VEVs determined by the standard method are evaluated in the tree-level plus one-loop potential minima; as a result, those results are gauge-dependent. Extending above to our model, the ξ dependence of $V_1(\phi, \phi_S, \xi)$ disappears while we evaluate T_C at the tree-level minima: $(\phi = v^{\text{tree}} = 246 \text{ GeV}, \phi_S = 0)$ and $(\phi = 0, \phi_S = v_S^{\text{tree}} = \sqrt{\mu_S^2/\lambda_S})$. For the two-step EWPT, the gauge-independent T_C can be obtained from the following:

$$\begin{aligned} & V_0(v^{\text{tree}}, 0) + V_{\text{CW}}(v^{\text{tree}}, 0) + V_1^T(v^{\text{tree}}, 0, T_C) \\ & = V_0(0, v_S^{\text{tree}}) + V_{\text{CW}}(0, v_S^{\text{tree}}) + V_1^T(0, v_S^{\text{tree}}, T_C). \end{aligned} \quad (2.38)$$

Note that as we are working on $\mathcal{O}(\hbar)$, the thermal resummation, a two-loop order $\mathcal{O}(\hbar^2)$ effect, is not performed. Going beyond $\mathcal{O}(\hbar)$ requires two-loop contributions which is out of scope of our current analysis. In the Appendix E, we give an example to explicitly show how the gauge dependence disappears when the potential is evaluated at the tree-level minima.

The minima, v_C and v_{SC} , are inherited gauge dependence which can easily be understood from the NFK identity: in Eq. (2.33), the field value minimizing the effective potential is gauge-dependent. To get gauge invariant VEVs in the PRM scheme, we have to utilize the HT potential, Eq. (2.32), by finding the minima at T_C , *i.e.*, find the minima of $V^{\text{HT}}(\phi, \phi_S, T_C)$.



Chapter 3

Numerical Analysis

In our model, m_S , λ_S and λ_{HS} are the free parameters. We take $m_S = m_H/2$ which is within DM experiment bound and phenomenology (see Sec. ?? for the discussion), and choose $\lambda_S = \lambda_S^{\min} + 0.1$, see Eq. (2.8); thus only λ_{HS} is varied in the analyses. Aiming to investigate the gauge dependence, a range of λ_{HS} is selected where the tree-level potential is relatively minor compared with gauge loop contributions to the potential barrier. Furthermore, this particular range meets the conditions of the two-step strong first-order EWPT ($v_C/T_C \simeq 1$ and several inequalities in Sec. 2.3.1). For clarity, our input parameters are listed in Table 3.1, and we summarize the settings of the each scheme in Table 3.2.

In Sec. 3.1, we list a detail procedure of finding T_C and v_C ; in addition, their precisions in the analyses are also shown. Our analyses can be divided into two parts: Sec. 3.2 focuses on the effect of gauge and the NG boson channels in the OS-like scheme, Sec. 3.3 demonstrates how the scheme dependence influences the results.

	Parameter				
	m_H	v_0	m_W	m_Z	m_t
Value [GeV]	125	246	80.4	91.1	173.2

Table 3.1: The input parameters in all schemes. Note that, besides the $\overline{\text{MS}}$ scheme (see Sec. 2.2), μ_H , μ_S , and λ_H satisfy the tree-level relations: $\mu_H^2 = m_H^2/2$, $\mu_S^2 = -m_S^2 + \lambda_{HS}/2v_0^2$ and $\lambda_H = m_H^2/2v_0^2$.

	OS-like	Scheme		
		$\overline{\text{MS}}$	HT	PRM
Tadpole Condition	Tree	1-loop	Tree	Tree
NG resummed	✓	-	-	-
Thermal resummed	✓	✓	-	-
ξ dependence	✓	✓	-	-



Table 3.2: Summary of the scheme settings.

3.1 Critical Temperature and Critical VEV

Two s of method of finding T_C are used; For the PRM scheme, T_C is found by Eq. 2.38. For the OS-like, the HT and the PRM schemes, T_C is searched by the bisection method whose details of procedure are listed in the following*:

1. choose two initialized temperatures, T_{\max} (*e.g.*, 200 GeV) and T_{\min} (100 GeV). To use the bisection method, one also needs a middle value, $T_{\text{mid}} = (T_{\max} + T_{\min})/2$ (150 GeV),
2. calculate the energy difference, ΔE , between the potential energy of minima in singlet's, $E(\phi^{\min})$, and doublet's, $E(\phi_S^{\min})$, directions[†] at T_{mid} , *i.e.*,

$$\Delta E(T_{\text{mid}}) = E(\phi^{\min}, T_{\text{mid}}) - E(\phi_S^{\min}, T_{\text{mid}}), \quad (3.1)$$

3. calculate ΔE at T_{\min} , that is

$$\Delta E(T_{\min}) = E(\phi^{\min}, T_{\min}) - E(\phi_S^{\min}, T_{\min}), \quad (3.2)$$

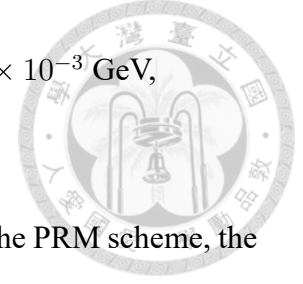
4. if $\Delta E(T_{\text{mid}}) \times \Delta E(T_{\min}) < 0$, we can redefine $T_{\min} \rightarrow T_{\text{mid}}$, and $T_{\max} \rightarrow T_{\text{mid}}$, otherwise $T_{\min} \rightarrow T_{\text{mid}}$ and $T_{\max} \rightarrow T_{\max}$,
5. take the new T_{mid} and T_{\min} back to the step 2. and go though the procedure again.

The above is calculated iteratively until

*We use Mathematica to analyse our model.

†We use the Findminimum, the optional methods InteriorPoint and PrincipleAxis are chose.

- $\Delta E(T_{\text{mid}})$ is less than 10^3 GeV,
- and the absolute temperature difference ($|T_{\text{mid}} - T_{\text{min}}|$) is $< 5 \times 10^{-3}$ GeV,
- or the maximum calculation count (20) is reached.



Then we regard T_{mid} as T_C ; v_C are searched in this temperature. For the PRM scheme, the gauge-invariant v_C is found by using Eq. (2.32) at T_C which is obtained from Eq. (2.38). In the Fig. 3.1, we show an example of the contour plots of the HT potential in the plane of $\langle \phi \rangle$ and $\langle \phi_S \rangle$ for temperatures are high, above, equal and below T_C ; zero temperature one is also included. All the parameters are chose to be $m_S = m_H/2$ and $\lambda_{HS} = 0.4$.

3.2 (non)Thermal Gauge and NG Boson Contribution

To numerically quantify the effect of gauge and NG boson contributions, we use several approximations by turning off specific channel to study the EWPT, see Fig. 3.2. “(T)GB off”, depicted by the (red) green (dot-dashed) dashed line, is denoted the computation without (thermal) non-thermal gauge boson contributions; “NG off”, depicted by the yellow dotted line, stands for NG boson contributions is omitted. “full”, depicted by the blue solid line, includes all the contributions. The left and right panels show T_C and v_C/T_C as functions of λ_{HS} , respectively.

Our results indicate that, in the range of $0.2 < \lambda_{HS} < 0.4$, the thermal gauge loop have a $\sim 11\%$ effect on T_C and $\sim 13\%$ on v_C/T_C . As mentioned before, the result is not precisely equivalent to the effect of ξ dependence. However, it demonstrates how gauge boson contributions affect the EWPT; thus, the gauge artifact should have large impact on the EWPT as well. Furthermore, [24] found that even though the percentage of difference is small in T_C as changing different ξ , it cannot guarantee that the dependence on gravitational waves generated from the first-order of EWPT is insignificant. In fact, by varying ξ from 0 to 5, the gravitational wave spectrum in a $U(1)_{B-L}$ model can change by one order of magnitude [24]. Above result indicates the necessity of quantification of the ξ dependence by using general R_ξ gauge which should be studied and noticed in the future.

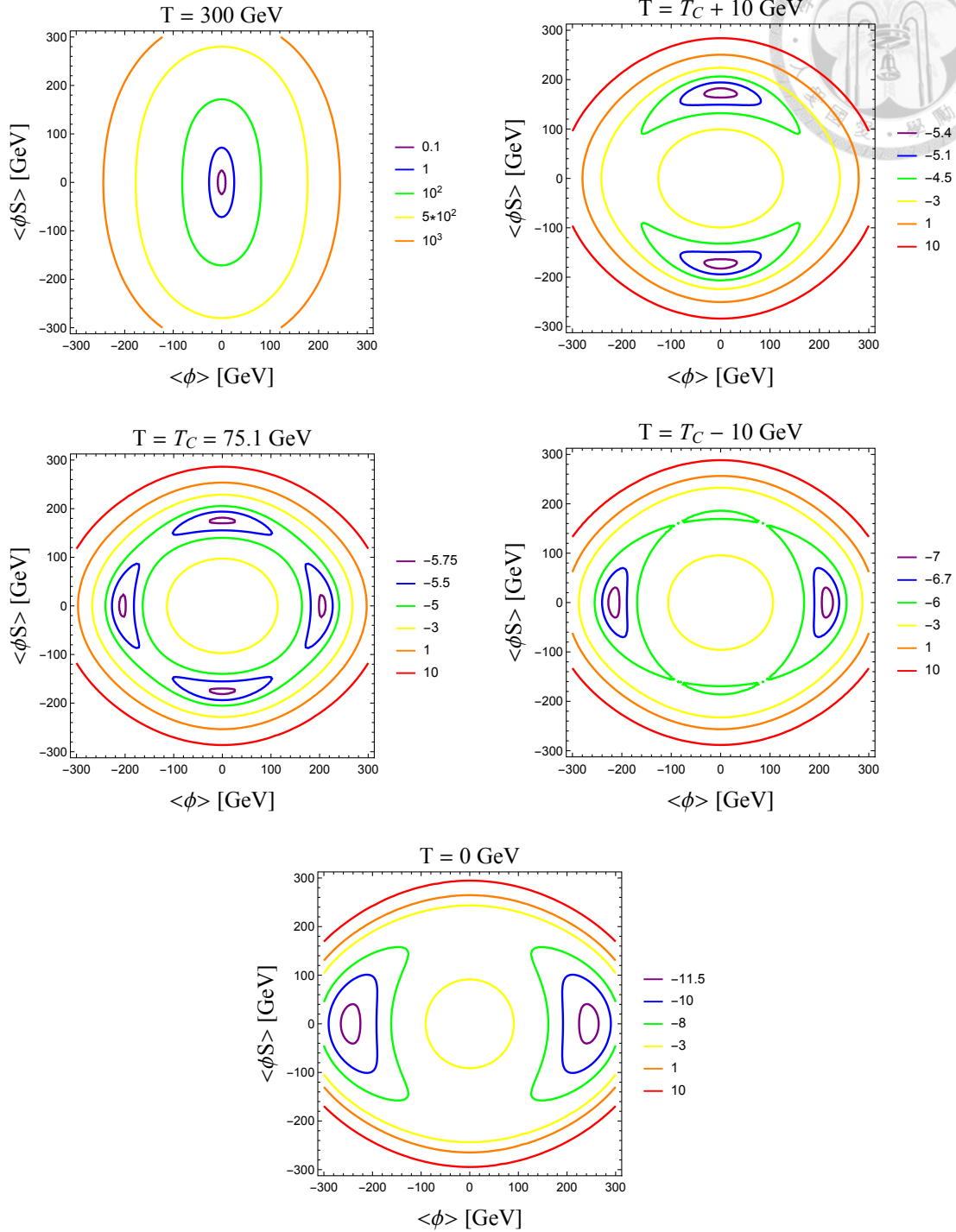


Figure 3.1: The contour plots of the HT effective potential in the plane of $\langle\phi\rangle$ and $\langle\phi_S\rangle$ at $T = 300$ GeV (Upper Left), $T = T_C + 10$ GeV (Upper Right), $T = T_C = 75.1$ GeV (Middle Left), $T = T_C - 10$ GeV (Middle Right) and $T = 0$ GeV (Lower). The parameters are, $m_S = m_H/2$ and $\lambda_{HS} = 0.4$. Note that all the plot legends are in the unit of 10^7 GeV.

In the NG off case, their effects are expected to be minor because that they are the two-loop level effects. However, when $\lambda_{HS} \lesssim 0.21$ where the thermal gauge loop dominates over the barrier compared with the tree-level contributions, NG boson effects are pronounced. To be noted that, in this region, the global minimum at T_C is no longer located on the doublet Higgs; instead, it is mixed with the doublet and the singlet contributions; this causes the downward curve of v_C/T_C . The (0.03 – 2.3)% difference is found in T_C , and (3.0 – 16.7)% in v_C/T_C . See the Table. 3.3 for the summary.

Channel	T_C	v_C/T_C
GB off	0.16 – 0.18	0.29 – 0.47
TGB off	11.4 – 11.8	11.7 – 16.8
NG off	0.03 – 2.3	3.0 – 16.7

Table 3.3: The percentage of the effects on the EWPT by turning off specific channel.

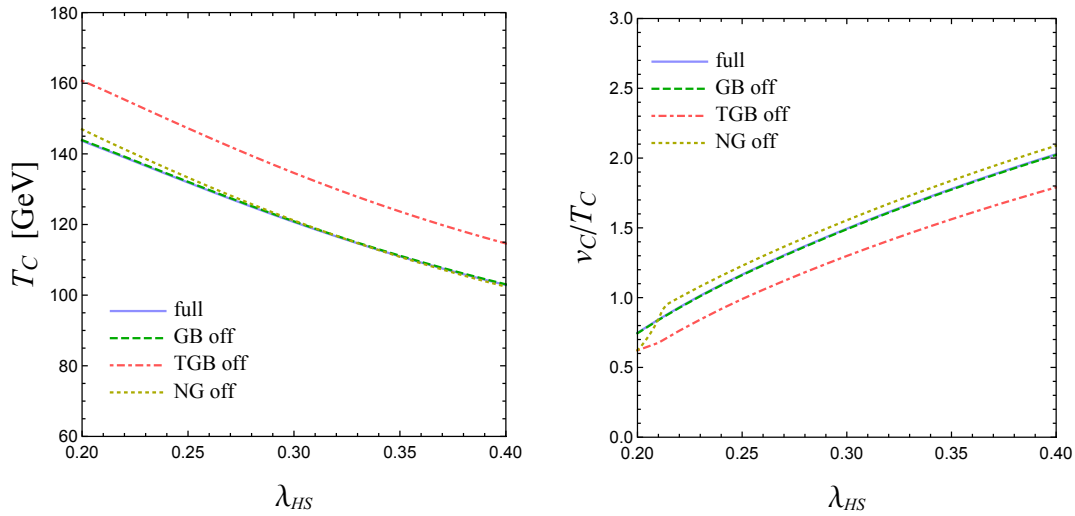


Figure 3.2: The effect of thermal (TGB off, red dot-dashed), non-thermal gauge (GB off, green dashed) and NG bosons (NG off, yellow dotted) contributions on T_C (Left panel) and v_C/T_C (Right panel) in the OS-like scheme. The blue solid line includes all the contributions.

3.3 Scheme Dependence Comparison

The scheme dependence, see Fig. 3.3, is studied by comparison between the \overline{MS} (green), the HT (black dotted) and the PRM (red) schemes. Since in the PRM and the \overline{MS} schemes

their zero-temperature one-loop potentials are scale-dependent, we vary the renormalization scale from $2m_t$ (solid) to $m_t/2$ (dashed), see Sec. 3.4 for more discussion.

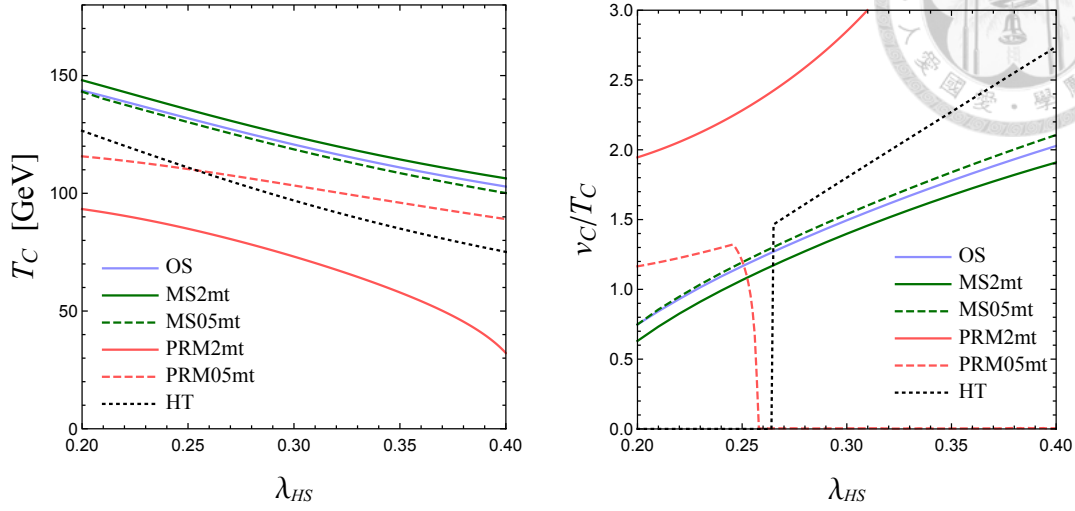


Figure 3.3: Comparison of scheme-dependent results and investigation of scale dependence. *Left*: Critical temperature as the function of λ_{HS} . *Right*: v_C/T_C as the function of λ_{HS} . The OS-like scheme with NG resummation and the HT scheme are depicted as the blue solid and black dotted lines, respectively. For the $\overline{\text{MS}}$ and the PRM schemes, the style of lines are green and red, respectively. In the legend, “MS2mt (MS05mt)” represents that the $\overline{\text{MS}}$ scheme’s renormalization scale is at $2m_t$ ($m_t/2$). Same notation is also applied to the PRM scheme.

We have the following results:

- The OS-like and the $\overline{\text{MS}}$ schemes have a nice agreement on each other as varying the renormalization scale. For T_C and v_C/T_C , $(0.4 - 3.4)\%$ and $(0.03 - 15)\%$ differences are found, respectively. When the $\overline{\text{MS}}$ scheme’s renormalization scale is taken as $m_t/2$, their results are closer. However, the large scale dependence demonstrates the necessity of the high-order corrections.
- The critical temperature in the HT scheme are observed to be smaller than the OS-like and the $\overline{\text{MS}}$ schemes by $10 \sim 30$ GeV. Furthermore, we find that when $\lambda_{HS} \lesssim 0.26$, the EWPT is not the first order: detail examination reveals that the energy degenerated minima on the doublet and singlet directions are saddle points; the global minimum is between the two axes. In addition, in the region where the first order PT is achieved, v_C/T_C is overestimated compared with the two other schemes.

- The PRM scheme shows a qualitatively consistency to the OS-like and the $\overline{\text{MS}}$ schemes in the behavior of T_C against λ_{HS} ; namely, as λ_{HS} decreases, T_C increases. Notice that one of the universal features of this scheme is that T_C is lower than the results from the stand method (Sec. 2.3.1); this is mainly because that the potential energy at the tree-level minimum is usually greater than the potential energy at the tree-level plus one-loop minimum. Therefore, T_C in Eq. (2.38) is lower than T_C in Eq. (2.28). Because T_C is relatively small, v_C/T_C is enhanced compared with the OS-like and the $\overline{\text{MS}}$ schemes. The reason of the downward curve in $\bar{\mu} = m_t/2$ at $\lambda_{HS} \gtrsim 0.25$ is because v_C in the PRM scheme is determined by the HT potential: When T_C is determined by Eq. 2.38 is higher than T_C in the HT scheme, it means that v_C must be zero at the HT potential; since the global minimum is moved to the singlet direction.

In general, no significant inconsistency between the results of the PRM scheme and other schemes are found. Their differences are within the theoretical uncertainty. For the quantitative analysis, higher-order correction such as $\mathcal{O}(\hbar^2)$ and the daisy improved calculations are needed in the future for the complete comparison.

3.4 Scale Dependence of T_C

The reason of appearing scale dependence of critical temperature is due to the method of determining T_C is at the one-loop level. In the PRM scheme, the tree-level tadpole conditions are used in the one-loop level in order to satisfy the NFK identity; thus, large $\bar{\mu}$ dependences appear in those schemes. This issue is relatively alleviated in the $\overline{\text{MS}}$ scheme: The reason is because the tadpole conditions of the $\overline{\text{MS}}$ scheme are set at the one-loop level. Hence, the $\bar{\mu}$ dependences of V_{CW} are partially cancelled. In the Fig. 3.4, we show the $\bar{\mu}$ dependence of T_C explicitly in the range of $2m_t \sim m_t/2$ while the $\lambda_{HS} = 0.2$. We find a spike at $\bar{\mu} \sim 109$ GeV and suspect this is purely caused by the accidental cancellation in V_{CW} among different particle contributions. Because the value of renormalization scale in denominator of logarithm can be larger or smaller than field-dependent masses in

numerator, this decreases the overall potential and needs larger thermal contributions to satisfy the degenerated condition.

Like shown in [25], one is possible to make T_C to be $\bar{\mu}$ -independent by replacing the parameters in the tree-level potential with running ones, *i.e.*, using renormalization group equations to evaluate the parameters. However, the starting scale of the running is still a input parameter. The fundamental solution of $\bar{\mu}$ dependences is to include the higher order correction which is beyond our current goal.

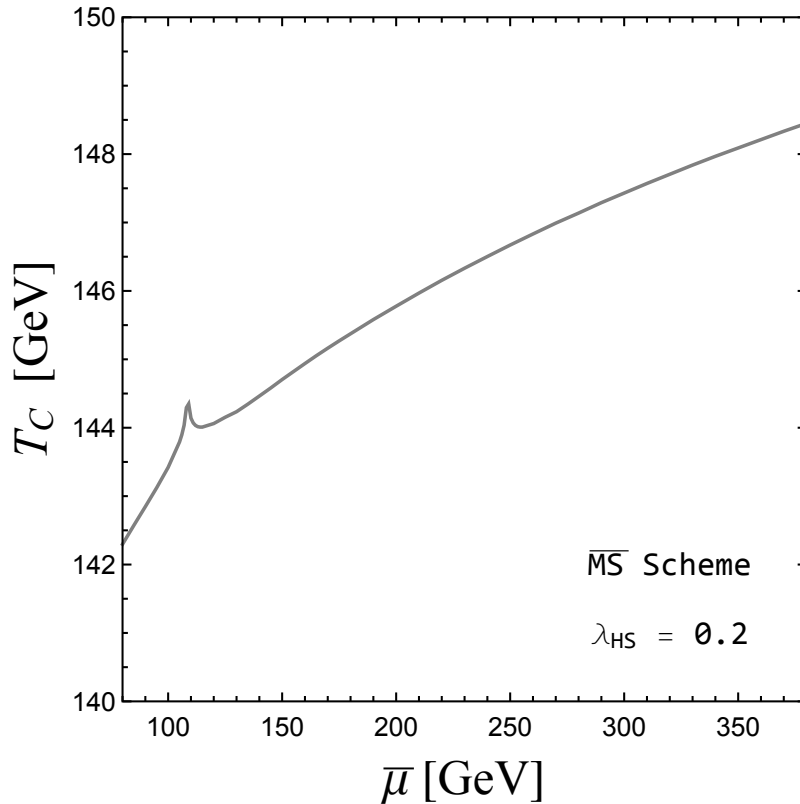


Figure 3.4: Critical temperature as the function of renormalization scale in the $\overline{\text{MS}}$ scheme. The parameter settings are $\lambda_{HS} = 0.2$ and $m_S = m_H/2$. The spike around 109 GeV is expected to be an accidental cancellation among contributions of different particle contents, not any physical or theoretical interest.



Chapter 4

Discussion and Conclusion

4.1 Discussion: Dark Matter, Vacuum Stability and Perturbativity

By imposing Z_2 symmetry, S can be one of the components of the dark matter [8, 9]. The parameters ($\lambda_{HS} = 0.2 - 0.4, m_S = m_H/2$) we chose is capable of escaping both the direct [26] and indirect detections [27]. It has been showed that, in the singlet DM model while DM mass is half of the Higgs mass, to achieve the relic density observed today ($\Omega h^2 = 0.1186 \pm 0.0020$) [28], λ_{HS} has to below 2×10^{-4} [29]. In our parameter region, the singlet DM contributes very little to the relic density ($3.29 \times 10^{-7} - 8.4 \times 10^{-8}$ calculated by `MicrOMEGAs 5.0.6`. [30]). However, if m_S is around 0.4 TeV, it is possible to generate the observed relic density.

Another issue in the resonance region ($m_S = m_H/2$) is that the small m_S is not able to keep the stability of the absolute vacuum when running the coupling to high energy scale (in the other words, the EW vacuum in this case is metastable) [31]; though in such scenario the life time of tunnelling to global minimum is still longer than the age of the universe. If m_S is 0.1 - 1 TeV with $\lambda_{HS} \gtrsim 0.2$, the Higgs quartic coupling will stay positive and it guarantees the stability. Even though high mass region can solve previous two issues (vacuum stability and insignificant contribution to relic density), λ_{HS} in those parameter space easily violates perturbativity calculation before the scale reaches the Planck scale

($\sim 10^{19}$ GeV). In contrast, the energy scale of perturbativity violation for our parameter settings can be very high [31]. In the most EWBG scenarios, they encounter the Landau pole before the scale reaches to the Planck scale while requiring the baryon preservation criterion $v_C/T_C \gtrsim 1$. In our case, for $\lambda_{HS} \lesssim 0.33$, all the couplings are below the 4π all the way to the Planck scale by using the one-loop renormalization group equations.

4.2 Conclusion

EWPT is revisited with the scalar singlet-extended SM by using several calculation schemes. The effect of thermal, non-thermal gauge channels and NG resummation are studied. The parameters space we investigate is $m_S = m_H/2$ and $0.2 \leq \lambda_{HS} \leq 0.4$.

In the OS-like scheme, the occurrence of the IR divergent in the NG boson channels demonstrates that the NG resummation is necessary; even though the NG resummation is the two-loop effect which is expected to be minor. We find that the NG resummation has a (0.03 – 2.3)% effect on T_C and (3.0 – 16.7)% on v_C/T_C . When the non-thermal gauge channels are turned off, small numerical impacts on T_C (0.16 – 0.18%) and v_C/T_C (0.29 – 0.47%) are observed. The effect of thermal gauge channels is relatively significant even when the tree barrier is present, (11.4 – 11.8)% on T_C and (11.7 – 16.8)% on v_C/T_C are detected. The above results have motivated us to investigate and quantify the ξ dependence by using the general R_ξ in a future work.

We find that both T_C and v_C/T_C in the OS-like and the $\overline{\text{MS}}$ schemes have nice agreement on each other; the differences are within the scale uncertainty. For T_C , their difference is (0.4 – 3.2)% and for v_C/T_C is (0.03 – 15)%. In the analysis between gauge-dependent and -independent schemes, we find that i) the HT scheme is over-simplified and T_C is largely underestimated, and ii) we find that the PRM scheme is qualitatively consistent to the OS-like and the $\overline{\text{MS}}$ schemes. However, the large theoretical uncertainties caused by renormalization scale demonstrates the higher order corrections are needed.



Appendix A

Generating Functional of 1(not 1)-PI

The effective action can generate 1PI correlation functions. To see this, we first begin by the second derivative of the generating functional for the connected Green's functions ($W[J]$):

$$\begin{aligned} \frac{\delta^2 W[J]}{\delta J(y) \delta J(z)} &= \hat{N} \int D\phi \phi(y) \exp\left(i \int \mathcal{L} + J\phi\right) \phi(z) \\ &\quad - \hat{N} \int D\phi \phi(y) \exp\left(i \int \mathcal{L} + J\phi\right) \times \hat{N} \int D\phi \phi(z) \exp\left(i \int \mathcal{L} + J\phi\right), \\ \text{where } \hat{N}^{-1} &= \int D\phi \exp\left(i \int \mathcal{L} + J\phi\right), \end{aligned} \tag{A.1}$$

where we have omitted the position variable in the parentheses. Above can be simplified by using Eq. (1.5) notation (the subscript, J , is omitted for simplicity),

$$\frac{\delta^2 W[J]}{\delta J(y) \delta J(z)} = \langle 0 | \phi(y) \phi(z) | 0 \rangle - \langle 0 | \phi(y) | 0 \rangle \langle 0 | \phi(z) | 0 \rangle. \tag{A.2}$$

The physical meaning of the above can be shown diagrammatically, the first term in the right hand side includes both*

$$x \text{ --- } \textcircled{\text{---}} \text{ --- } y, \tag{A.3}$$

*Diagrams are generated by [32].

$$x - \text{blob} + \text{blob} - y, \quad (\text{A.4})$$

where every blob contains sum of connect diagrams. For the second term of Eq. (A.2), it contains only diagrams like Eq. (A.4). Thus, $W[J]$ generates diagrams like Eq. (A.3) alone; furthermore, the higher derivatives of $W[J]$ will still generate the connect diagrams as desired. The effective action generates **the inverse** of the same two-point diagrams as $W[J]$. To see this, from Eq. (1.9), we know that

$$-\delta(x - y) = \frac{\delta}{\delta J(y)} \frac{\delta \Gamma[J]}{\delta \phi_c(x)} = \int d^4 z \frac{\delta \phi_c(z)}{\delta J(y)} \frac{\delta^2 \Gamma[J]}{\delta \phi_c(x) \delta \phi_c(z)}. \quad (\text{A.5})$$

Furthermore, substituting ϕ_c with Eq. (1.5), we have

$$-\delta(x - y) = \int d^4 z \frac{\delta^2 W[J]}{\delta J(y) \delta J[z]} \frac{\delta^2 \Gamma[J]}{\delta \phi_c(x) \delta \phi_c(z)}, \quad (\text{A.6})$$

one can easily observe that the second derivative of the effective action is actually the inverse of the two point function. At this point, one can already notice that the generating function of the effective action; however, to demonstrate the ability of generating 1PI, one has to go to the 3rd or higher derivative of the effective action. Before showing the main difference of $\Gamma[\phi_c]$ and $W[J]$, we first consider

$$\begin{aligned} \frac{\delta}{\delta J[Z]} &= \int d^4 w \frac{\delta \phi_c(w)}{\delta J(z)} \frac{\delta}{\delta \phi_c(w)} = -i \int d^4 w D(z, w) \frac{\delta}{\delta \phi_c(w)}, \\ \text{where } -iD(z, w) &= \frac{\delta^2 W[j]}{\delta J[z] \delta J[w]} = \left(\frac{\delta^2 \Gamma[\phi_c]}{\delta \phi_c(z) \delta \phi_c(w)} \right)^{-1}. \end{aligned} \quad (\text{A.7})$$

The 3rd derivative of $W[J]$ is then

$$\frac{\delta^3 W[z]}{\delta J(x) \delta J(y) \delta J(z)} = i \int d^4 w D(z, w) \frac{\delta}{\delta \phi_c(w)} \left(\frac{\delta^2 \Gamma[\phi_c]}{\delta \phi_c(x) \delta \phi_c(y)} \right)^{-1}, \quad (\text{A.8})$$

to evaluate the derivative of the parentheses we use

$$\frac{\partial}{\partial \alpha} \mathbf{M}^{-1}(\alpha) = -\mathbf{M}^{-1} \frac{\partial \mathbf{M}(\alpha)}{\partial \alpha} \mathbf{M}^{-1}. \quad (\text{A.9})$$

Consequently, we have

$$\begin{aligned}
 \frac{\delta^3 W[z]}{\delta J(x)\delta J(y)\delta J(z)} &= -i \int d^4 w D(z, w) \\
 &\int d^4 u d^4 v \left(\frac{\delta^2 \Gamma}{\delta \phi_c(x)\phi_c(u)} \right)^{-1} \frac{\delta^3 \Gamma}{\delta \phi_c(u)\delta \phi_c(v)\delta \phi_c(w)} \left(\frac{\delta^2 \Gamma}{\delta \phi_c(v)\phi_c(y)} \right)^{-1}, \\
 &= i \int d^4 w d^4 u d^4 v D(z, w) D(x, u) \frac{\delta^3 \Gamma}{\delta \phi_c(u)\delta \phi_c(v)\delta \phi_c(w)} D(v, y),
 \end{aligned}
 \tag{A.10}$$

where in the last step, Eq. (A.7) is used. The equation can be understood by the digram again:

$$z \text{---} \text{shaded circle} \text{---} x \text{---} y = z \text{---} \text{shaded circle} \text{---} w \text{---} \text{crossed dot} \text{---} v \text{---} y, \tag{A.11}$$

where the left hand side digram equals to the 3rd derivative of $W[J]$; the two-point functions connect the internal positions u, v and w , which will be integrated out later, to the external points (x, y and z). In the right hand side, the crossed dot which connects the the internal positions represents the 3rd derivative of the effective action; since the external lines are amputated, one can observe that the crossed dot is actually a 1PI three-point function which is generated by the effective action. Additionally, one can show that for $n \geq 3$, the effective action is the generating functional for 1PI n -point Green's function.



Appendix B

Effective Potential in One-Loop

To calculate the one-loop effective potential, recall the general form, Eq. (1.24), for convenience,

$$V_1(\phi_c) = -\frac{i}{2} \int \frac{d^4 p}{(2\pi)^4} \text{Tr} \ln iG^{-1}(p; \phi_c). \quad (\text{B.1})$$

We first consider a simple theory with a scalar field, where its Lagrangian is given by

$$\begin{aligned} \mathcal{L} &= \frac{1}{2} (\partial_\mu \phi(x))^2 - \frac{1}{2} m^2 \phi^2(x) - \frac{\lambda}{4!} \phi^4(x), \\ \text{and } V_0 &= \frac{1}{2} m^2 \phi^2(x) + \frac{\lambda}{4!} \phi^4(x). \end{aligned} \quad (\text{B.2})$$

The propagator of this theory is then

$$G(p; \phi_c) = \frac{i}{p^2 - m^2(\phi_c) + i\epsilon}, \quad (\text{B.3})$$

where the definition of $m(\phi_c)$ can be found in Appendix D while λ_{HS} is turned off. Since the scalar field is absent of internal d.o.f., the trace in Eq. (B.1) is equal to 1; so that it becomes

$$V_1(\phi_c) = -\frac{i}{2} \int \frac{d^4 p}{(2\pi)^4} \ln (p^2 - m^2(\phi_c) + i\epsilon). \quad (\text{B.4})$$

In order to evaluate the integral, a Wick rotation is performed:

$$\begin{aligned} V_1(\phi_c) &= \frac{1}{2} \int \frac{d^4 p_E}{(2\pi)^4} \ln(p_E^2 + m^2(\phi_c)), \\ \mu^\varepsilon V_1(\phi_c) &= \frac{1}{2} \mu^\varepsilon \int \frac{d^D p_E}{(2\pi)^D} \ln(p_E^2 + m^2(\phi_c)), \end{aligned} \quad (\text{B.5})$$



where we have suppressed the $i\epsilon$ term and subtracted a constant coefficient, $\ln(-1)$. In the second equality, we have used the dimension regularization. In the D -dimension, λ has the dimension of $4 - D \equiv \varepsilon$; however, instead of using a non-integral dimensional coupling constant, we introduce a parameter (μ), which later is recognized as a renormalization scale and it has mass dimension, and trade $\lambda \rightarrow \lambda\mu^\varepsilon$. To unfold the logarithm, one has to calculate the derivative with respect to m^2 ,

$$\begin{aligned} \mu^\varepsilon \frac{\partial V_1(\phi_c)}{\partial m^2(\phi_c)} &= \frac{1}{2} \mu^\varepsilon \int \frac{d^D p_E}{(2\pi)^D} \frac{1}{p_E^2 + m^2(\phi_c)}, \\ &= \frac{1}{2} \mu^\varepsilon \frac{1}{(4\pi)^{D/2}} \frac{1}{(m^2(\phi_c))^{1-D/2}} \Gamma\left(1 - \frac{D}{2}\right), \end{aligned} \quad (\text{B.6})$$

where the identity [33],

$$\int \frac{d^D k}{(2\pi)^D} \frac{k^{2a}}{(k^2 - \Delta)^b} = i(-1)^{a-b} \frac{1}{(4\pi)^{d/2}} \frac{1}{\Delta^{b-a-d/2}} \frac{\Gamma(a + \frac{b}{2}) \Gamma(b - a - \frac{d}{2})}{\Gamma(b) \Gamma(\frac{d}{2})}, \quad (\text{B.7})$$

has been used. Integrating with respect to m^2 ,

$$\begin{aligned} \mu^\varepsilon V_1(\phi_c) &= \frac{1}{2} \mu^\varepsilon \frac{1}{(4\pi)^{D/2}} \Gamma\left(1 - \frac{D}{2}\right) \frac{2}{D} (m^2)^{D/2}, \\ &= \frac{1}{32\pi^2} \left(\frac{m^2}{4\pi\mu^2}\right)^{D/2-2} \Gamma\left(1 - \frac{D}{2}\right) \frac{2m^4}{D}, \\ &= -\frac{m^4}{32\pi^2} \frac{1}{\frac{D}{2}(\frac{D}{2}-1)} \left(\frac{m^2}{4\pi\mu^2}\right)^{D/2-2} \Gamma\left(2 - \frac{D}{2}\right), \\ &= -\frac{m^4}{64\pi^2} \left(1 + \frac{3}{4}\varepsilon + \mathcal{O}(\varepsilon^2) + \dots\right) \left(1 - \frac{\varepsilon}{2} \ln \frac{m^2}{4\pi\mu^2} + \mathcal{O}(\varepsilon^2) + \dots\right) \\ &\quad \times \left(\frac{2}{\varepsilon} - \gamma_E + \mathcal{O}(\varepsilon) + \dots\right), \\ &= \frac{m^4}{64\pi^2} \left(-\frac{2}{\varepsilon} - \ln 4\pi + \gamma_E + \ln \frac{m^2}{\mu^2} - \frac{3}{2} + \mathcal{O}(\varepsilon^2) + \dots\right), \end{aligned} \quad (\text{B.8})$$

where we have used the Γ function's property: $\Gamma(1+z) = z\Gamma(z)$. Taylor expansions have also been performed; thus after utilizing the $\overline{\text{MS}}$ renormalization scheme (we also present $\overline{\text{DR}}$ scheme for the completeness. In this case, these two schemes give the same results.) and taking $\varepsilon \rightarrow 0$, we have

$$V_1^{\text{scalar}}(\phi_c) = \frac{m^4(\phi_c)}{64\pi^2} \left(\ln \frac{m^2(\phi_c)}{\bar{\mu}^2} - \frac{3}{2} \right), \quad (\overline{\text{MS}}\text{-scheme} = \overline{\text{DR}}\text{-scheme}), \quad (\text{B.9})$$

where $\bar{\mu}^2 = 4\pi e^{-\gamma_E} \mu^2$. Notice that in the following, we adopt procedures that i) the dimensional regularization scheme is followed by the $\overline{\text{MS}}$ renormalization scheme; ii) the dimensional reduction is renormalized by the $\overline{\text{DR}}$ scheme. In the thesis, we use the former method.

For fermion, the relevant part of Lagrangian is

$$\mathcal{L}(\phi, \psi) \sim \bar{\psi} (\not{\partial} - m_f(\phi_c)) \psi, \quad (\text{B.10})$$

and its propagator is

$$G_f = \frac{i}{p^2 - m_f^2(\phi_c) + i\epsilon}. \quad (\text{B.11})$$

Note that only diagrams with even number of vertexes have contributions, since the trace of odd number gamma matrix(s) is zero. The internal d.o.f. of fermion is the spinor space whose trace actually is depended on the regularization schemes,

$$\text{Tr}(\mathbf{1}) = \begin{cases} 2^{D/2} = 2^{\varepsilon/2-2}, & \text{dimensional regularization,} \\ 4, & \text{dimensional reduction.} \end{cases} \quad (\text{B.12})$$

Accordingly, the one-loop potential for fermion case is then

$$V_1(\phi_c) = \frac{i}{2} \int \frac{d^4 p}{(2\pi)^4} \text{Tr}(\mathbf{1}) \text{Tr} \ln(p^2 - m_f^2(\phi_c)), \quad (\text{B.13})$$

where the addition minus comes from the fermionic loop; the second trace is for the different fermion species. By performing the similar procedure like above, we have

$$V_1^{\text{fermion}}(\phi_c) = \begin{cases} -4 \times \frac{m_f^4(\phi_c)}{64\pi^2} \left(\ln \frac{m_f^2(\phi_c)}{\bar{\mu}^2} - \frac{3}{2} + \ln 2 \right), & (\overline{\text{MS}}\text{-scheme}), \\ -4 \times \frac{m_f^4(\phi_c)}{64\pi^2} \left(\ln \frac{m_f^2(\phi_c)}{\bar{\mu}^2} - \frac{3}{2} \right), & (\overline{\text{DR}}\text{-scheme}). \end{cases} \quad (\text{B.14})$$

Note that the factor, $\ln 2$, is often omitted in the convention, as it is absorbed in $\bar{\mu}$. If the perturbation is good enough, the small difference of $\bar{\mu}$ will not change the result significantly; we also mention how this issue affect T_C in the Sec. 3.4.

Above is also applied to the boson channels. For boson case, gauge bosons related parts in Lagrangian are

$$\mathcal{L}(\phi_c, A_\mu) \sim \frac{-1}{2} (F^{\mu\nu} F_{\mu\nu}) + \frac{1}{2} (\partial_\mu \phi_c)^\dagger \partial^\mu \phi_c + \frac{1}{2} (M_g^2)_{ab} A_\mu^a A^{b\mu} + \dots \quad (\text{B.15})$$

For $(M_g^2)_{ab}$, one can check Eq. (E.18). After taking the Landau gauge, the propagator is

$$G_g = \frac{i}{p^2 - M_g^2(\phi_c)} \Delta^{\mu\nu}, \quad (\text{B.16})$$

where $\Delta^{\mu\nu} = g^{\mu\nu} - p^\mu p^\nu / p^2$. The trace of the inverse propagator is

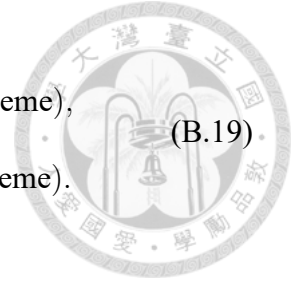
$$\text{Tr} (iG_g^{-1}) = \text{Tr} (p^2 - M_g^2(\phi_c)) \text{Tr} (\Delta^{\mu\nu}), \quad (\text{B.17})$$

where the first trace is for the different channels of the gauge bosons; the second trace is depended on regularization scheme:

$$\text{Tr} (\Delta^{\mu\nu}) = g_{\mu\nu} \Delta^{\mu\nu} \begin{cases} = D - 1 = 3 - \varepsilon, & \text{dimension regularization,} \\ = 3, & \text{dimension reduction.} \end{cases} \quad (\text{B.18})$$

Finally, the one-loop potential for gauge bosons are given by

$$V_1^{\text{boson}}(\phi_c) = \begin{cases} 3 \times \frac{M_g^4(\phi_c)}{64\pi^2} \left(\ln \frac{M_g^2}{\bar{\mu}^2} - \frac{5}{6} \right), & (\overline{\text{MS}}\text{-scheme}), \\ 3 \times \frac{M_g^4(\phi_c)}{64\pi^2} \left(\ln \frac{M_g^2}{\bar{\mu}^2} - \frac{3}{2} \right), & (\overline{\text{DR}}\text{-scheme}). \end{cases} \quad (\text{B.19})$$





Appendix C

Approximate Thermal Function

The thermal functions are infinite sums of modified Bessel functions of the second kind (K_2) [22]:

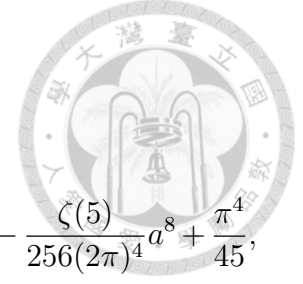
$$I_{B,F}(a^2) = -a^2 \sum_{n=1}^{\infty} \frac{(\pm 1)^2}{n^2} \Re K_2(na), \quad (\text{C.1})$$

where the plus and minus signs are for the boson and fermion, respectively. We set the goal of the difference between approximate functions and the numerical integrations should be less than 10^{-6} . To achieve this, we investigate the following:

C.1 Boson

In the region of $a = \bar{m}/T < 0.35$, we approximate the thermal function (I_B) with a high temperature expansion for boson (HTEB); in $0.35 \leq a \leq 9.0$, a polynomial fitting function for boson (PFFB) is used; a low temperature approximation for boson (LTEB) is adopted for $a > 9.0$; when $a \in i\Re$, we replace $\Re K_2$ with the second kind of unmodified Bessel function (Y_2) by an identity.

C.1.1 HTEB ($a < 0.35$)



The HTEB we adopt is [34]

$$-\frac{\pi^4}{45} + \frac{\pi^2}{12}a^2 - \frac{\pi}{6}(a^2)^{3/2} - \frac{a^4}{32} \left(\log(a^2) - 3.91 - \frac{3}{2} \right) + \frac{\zeta(3)}{96(2\pi)^2}a^6 - \frac{\zeta(5)}{256(2\pi)^4}a^8 + \frac{\pi^4}{45}, \quad (\text{C.2})$$

where ζ is the Riemann zeta function and the last term is for the normalization. Note that we truncate the expansion at $\mathcal{O}(a) = 8$, since the difference between the HTEB and the numerical integration, which is performed by the routine `NIntegrate` in `Mathematica`, is less than 1.2×10^{-6} .

C.1.2 PFFB ($0.35 \leq a \leq 9.0$)

Though the above HTEB is sufficient at $a < 0.35$, above this threshold, the HTEB needs to include more higher order terms. Instead, we adopt the PFFB for the middle temperature region, its detail form is the following:

$$\begin{aligned} & -1.3399397387595 \times 10^{-4} + 1.6469900315759 \times 10^{-3}a + 8.1272859398439 \times 10^{-1}a^2 \\ & - 4.7992824417603 \times 10^{-1}a^3 + 1.7878967977712 \times 10^{-1}a^4 - 6.0632418036213 \times 10^{-2}a^5 \\ & + 2.0900675811146 \times 10^{-2}a^6 - 6.5865607755012 \times 10^{-3}a^7 + 1.6413560386569 \times 10^{-3}a^8 \\ & - 2.7585765349357 \times 10^{-4}a^9 + 1.6331229085345 \times 10^{-5}a^{10} + 6.3995356651085 \times 10^{-6}a^{11} \\ & - 2.4477725951995 \times 10^{-6}a^{12} + 4.7496664471527 \times 10^{-7}a^{13} - 6.1710744609837 \times 10^{-8}a^{14} \\ & + 5.6506277097478 \times 10^{-9}a^{15} - 3.6262488646246 \times 10^{-10}a^{16} + 1.5599595264175 \times 10^{-11}a^{17} \\ & - 4.0517259606745 \times 10^{-13}a^{18} + 4.8112110679805 \times 10^{-15}a^{19}. \end{aligned}$$

The difference between the PFFB and the numerical integration is less than 1.5×10^{-7} as desired.

C.1.3 LTEB ($a > 9.0$)

We find that when $a > 9.0$, the deviation of the PFFB from the numerical integration is increasing as a is increasing, although the higher order terms are included. At this low temperature region, the LTEB is particular good compared with the PFFB. We truncated the LTEB at $\mathcal{O}(a) = 1/2$:

$$-\sqrt{\frac{\pi}{2}}a^{3/2}\left(\frac{105}{128a^2} + \frac{15}{8a} + 1\right)e^{-a} + \frac{\pi^4}{45}. \quad (\text{C.3})$$

The desired small difference (1.4×10^{-6}) between the LTEB and the numerical integration is achieved.

C.1.4 Bessel Approximation for $a \in i\Re$

The real part of the modified Bessel function of the second kind with the pure imaginary argument is proportional to the unmodified Bessel function of the second kind (Y_2), see [35, Eq. 9],

$$\Re K_2(bi) = \frac{\pi}{2}Y_2(b). \quad (\text{C.4})$$

A built-in function of Mathematica, `BesselY`, is used to evaluate Y_2 . The Bessel approximation we take is the following:

$$-a^2\frac{\pi}{2}\sum_1^m\frac{1^n}{n^2}Y_2(n \times \text{Im}(a)) + \frac{\pi^4}{45}. \quad (\text{C.5})$$

To save the computational time, we first create a table of a v.s. Eq. (C.5). The step of a in the table is 0.01, the range of a is from 0.01 to 100, and m is 1200. Since the `BesselY` cannot be well evaluated while $a = 0$, we set the function equals to zero while argument is zero. Finally, the table is fitted by the function, `Interpolation`. We use the resulting fitting function hereafter.

C.2 Fermion

Similar to the boson case, the high temperature expansion for fermion (HTEF) is used. Note that the threshold ($a < 0.32$) is different from the boson case; a polynomial fitting function for fermion (PFFF) is adopted in the range of $0.32 \leq a \leq 9.0$; the low temperature expansion for fermion (LTEF) is adopted when $a > 9.0$; when $a \in i\Re$, a Bessel approximation is same as the boson case except a factor, $(-1)^n$, and a normalization factor, $-7\pi^4/360$.

C.2.1 HTEF ($a < 0.32$)

The HTEF we utilize is

$$\frac{7\pi^4}{360} - \frac{\pi^2}{24}a^4 \left(\log(a^2) - 1.14 - \frac{3}{2} \right) + \frac{7\zeta(3)}{96(2\pi)^2}a^6 - \frac{31\zeta(5)}{256(2\pi)^4}a^8 + \frac{127\zeta(7)}{512(2\pi)^6}a^{10} - \frac{7\pi^4}{360}, \quad (\text{C.6})$$

where again ζ is the Riemann zeta function and the normalization is also added. The difference between the HTEF and the numerical integration is less than 1.5×10^{-6} . We find out that when $a > 0.32$, the difference is bigger than our precision goal.

C.2.2 PFFF ($0.32 \leq a \leq 9.0$)

Similar to the boson case, as a is greater than the threshold, the HTEF is insufficient. To be noted that the order of PFFF is different from PFFB ($\mathcal{O}(a) = 19$), we need less terms to achieve the precision goal:

$$\begin{aligned} & - 1.8606350459538 \times 10^{-4} + 2.1643938728080 \times 10^{-3}a - 4.2311984215163 \times 10^{-1}a^2 \\ & + 4.8651379062231 \times 10^{-2}a^3 + 8.4866222329381 \times 10^{-2}a^4 - 5.3476197518025 \times 10^{-2}a^5 \\ & + 1.7903012239488 \times 10^{-2}a^6 - 4.2239918118272 \times 10^{-3}a^7 + 7.8257512405354 \times 10^{-4}a^8 \\ & - 1.2116831287896 \times 10^{-4}a^9 + 1.6079151201184 \times 10^{-5}a^{10} - 1.7979838681990 \times 10^{-6}a^{11} \\ & + 1.6136414363595 \times 10^{-7}a^{12} - 1.0897600155288 \times 10^{-8}a^{13} + 5.1115038418446 \times 10^{-10}a^{14} \\ & - 1.4699419052289 \times 10^{-11}a^{15} + 1.9415262439880 \times 10^{-13}a^{16}. \end{aligned}$$

The difference between the PFFF and the numerical integration is less than 3×10^{-6} as desired.



C.2.3 LTEF ($a > 9.0$)

Again, the PFFF is merely sufficient when $a \sim 9.0$. In the low temperature region, the LTEF is relatively easy and precision-wise good:

$$\sqrt{\frac{\pi}{2}} a^{3/2} e^{-a} \left(1 + \frac{15}{8a} + \frac{105}{128a^2} \right) - \frac{7\pi^4}{360}. \quad (\text{C.7})$$

The difference between the LTEF and the numerical integration is less than 1.4×10^{-6} .

C.2.4 $a \in i\Re$

Similarly, when $a \in i\Re$, we use the identity Eq. (C.4),

$$-a^2 \frac{\pi}{2} \sum_1^m \frac{(-1)^n}{n^2} Y_2(n \times \text{Im}(a)) - \frac{7\pi^4}{360}, \quad (\text{C.8})$$

where $m = 1200$ and the procedure for creating fitting function is same as the boson case.



Appendix D

Field-Dependent Mass

D.1 Higgs Bosons

For the scalar sector, the mass matrix is

$$\begin{pmatrix} \partial V_0^2/\partial\phi^2 & \partial V_0^2/\partial\phi\partial\phi_S \\ \partial V_0^2/\partial\phi_S\partial\phi & \partial V_0^2/\partial\phi_S^2 \end{pmatrix} = \begin{pmatrix} -\mu_H^2 + 3\lambda_H\phi^2 + \lambda_{HS}\phi_S^2/2 & \lambda_{HS}\phi\phi_S \\ \lambda_{HS}\phi\phi_S & -\mu_S^2 + 3\lambda_S\phi_S^2 + \lambda_{HS}\phi^2/2 \end{pmatrix}, \quad (\text{D.1})$$

$$\equiv \begin{pmatrix} \bar{m}_{hh}^2 & \bar{m}_{hS}^2 \\ \bar{m}_{Sh}^2 & \bar{m}_{SS}^2 \end{pmatrix}. \quad (\text{D.2})$$

Changing to the physical-mass basis, the eigenvalues are,

$$\begin{aligned} \text{when } \bar{m}_{hh}^2 > \bar{m}_{SS}^2, & \begin{cases} \bar{m}_{H_1}^2(\phi, \phi_S) = \frac{1}{2} \left(\bar{m}_{hh}^2 + \bar{m}_{SS}^2 + \sqrt{(\bar{m}_{hh}^2 - \bar{m}_{SS}^2)^2 + 4\bar{m}_{hS}^4} \right), \\ \bar{m}_{H_2}^2(\phi, \phi_S) = \frac{1}{2} \left(\bar{m}_{hh}^2 + \bar{m}_{SS}^2 - \sqrt{(\bar{m}_{hh}^2 - \bar{m}_{SS}^2)^2 + 4\bar{m}_{hS}^4} \right), \end{cases} \\ \text{when } \bar{m}_{hh}^2 < \bar{m}_{SS}^2, & \begin{cases} \bar{m}_{H_2}^2(\phi, \phi_S) = \frac{1}{2} \left(\bar{m}_{hh}^2 + \bar{m}_{SS}^2 + \sqrt{(\bar{m}_{hh}^2 - \bar{m}_{SS}^2)^2 + 4\bar{m}_{hS}^4} \right), \\ \bar{m}_{H_1}^2(\phi, \phi_S) = \frac{1}{2} \left(\bar{m}_{hh}^2 + \bar{m}_{SS}^2 - \sqrt{(\bar{m}_{hh}^2 - \bar{m}_{SS}^2)^2 + 4\bar{m}_{hS}^4} \right). \end{cases} \end{aligned} \quad (\text{D.3})$$

Note that the above conventions make H_1 always be doublet-like and H_2 always be singlet-like. In the potential, the overall contributions of H_1 and H_2 should not be affected by the

conventions; however, in the NG resummation, the conventions are important for the first two terms in Eq. (2.17), as \bar{m}_{H_1} and \bar{m}_{H_2} are for doublet-like and singlet-like particles, specifically.

While considering the thermal corrected field-dependent masses, the mass matrix becomes

$$\begin{pmatrix} \bar{m}_{hh}^2 + \Sigma_H(T) & \bar{m}_{hS}^2 \\ \bar{m}_{Sh}^2 & \bar{m}_{SS}^2 + \Sigma_S(T) \end{pmatrix}, \quad (\text{D.4})$$

where

$$\Sigma_H(T) = \left(\frac{\lambda_H}{2} + \frac{\lambda_{HS}}{24} + \frac{3g_2^2 + g_1^2}{16} + \frac{y_t^2}{4} \right) T^2, \quad (\text{D.5})$$

$$\Sigma_S(T) = \left(\frac{\lambda_S}{4} + \frac{\lambda_{HS}}{6} \right) T^2. \quad (\text{D.6})$$

The eigenvalues are then

$$\begin{aligned} \bar{M}_{H_1, H_2}^2(\phi, \phi_S, T) = & \frac{1}{2} \left(\bar{m}_{hh}^2 + \bar{m}_{SS}^2 + \Sigma_H(T) + \Sigma_S(T) \right. \\ & \left. \pm \sqrt{(\bar{m}_{hh}^2 - \bar{m}_{SS}^2 + \Sigma_H(T) - \Sigma_S(T))^2 + 4\bar{m}_{hS}^4} \right). \end{aligned} \quad (\text{D.7})$$

The total effect of H_1 and H_2 to the thermal contributions will be summed up. Therefore, the role (the plus-minus sign) of H_1 and H_2 are relatively trivial.

D.2 NG Bosons

The field-dependent NG bosons take the form of

$$\bar{m}_{G^0}^2(\phi, \phi_S) = \bar{m}_{G^\pm}^2(\phi, \phi_S) = \frac{\partial^2 V_0}{\partial G^2} = -\mu_H^2 + \lambda_H \phi^2 + \frac{\lambda_{HS}}{2} \phi_S^2. \quad (\text{D.8})$$

The thermally corrected field-dependent masses will be

$$\bar{M}_{G^0}^2(\phi, \phi_S, T) = \bar{M}_{G^\pm}^2(\phi, \phi_S, T) = -\mu_H^2 + \lambda_H \phi^2 + \frac{\lambda_{HS}}{2} \phi_S^2 + \Sigma_H(T). \quad (\text{D.9})$$

D.3 Gauge Boson



For gauge bosons,

$$\overline{m}_W^2(\phi) = \frac{g_2^2}{4}\phi^2, \quad \overline{m}_Z^2(\phi) = \frac{g_2^2 + g_1^2}{4}\phi^2. \quad (\text{D.10})$$

For thermally corrected gauge bosons, in the transverse part, no static thermal mass is in the perturbation theory:

$$\overline{M}_{W_T}^2(\phi) = \overline{m}_W^2(\phi), \quad \overline{M}_{Z_T}^2(\phi) = \overline{m}_Z^2(\phi). \quad (\text{D.11})$$

Only the longitudinal part of gauge bosons require the thermal correction. The thermally corrected mass matrix in the basis $(A_\mu^1, A_\mu^2, A_\mu^3, B_\mu)$ is

$$\begin{pmatrix} g_2^2/4 + \Pi_W(T) & 0 & 0 & 0 \\ 0 & g_2^2/4 + \Pi_W(T) & 0 & 0 \\ 0 & 0 & g_2^2/4 + \Pi_W(T) & -g_2g_1\phi^2/4 \\ 0 & 0 & -g_2g_1\phi^2/4 & g_1^2/4 + \Pi_B(T) \end{pmatrix}. \quad (\text{D.12})$$

Eigenvalues of longitudinal parts are

$$\begin{aligned} \overline{M}_{Z_L, \gamma_L}^2(\phi, T) = & \frac{1}{2} \left(\frac{1}{4}(g_2^2 + g_1^2)\phi^2 + \Pi_W(T) + \Pi_B(T) \right. \\ & \left. \pm \sqrt{\left(\frac{1}{4}(g_2^2 - g_1^2)\phi^2 + \Pi_W(T) - \Pi_B(T) \right)^2 + \frac{g_2^2g_1^2}{4}\phi^4} \right), \end{aligned} \quad (\text{D.13})$$

$$\overline{M}_{W_L}^2(\phi, T) = \overline{m}_W^2(\phi) + \Pi_W(T), \quad (\text{D.14})$$

where

$$\Pi_W(T) = \left(\frac{5}{6} + \frac{N_g(N_C + 1)}{12} \right) g_2^2 T^2 \quad \underset{N_g=N_C=3}{=} \frac{11}{6} g_2^2 T^2, \quad (\text{D.15})$$

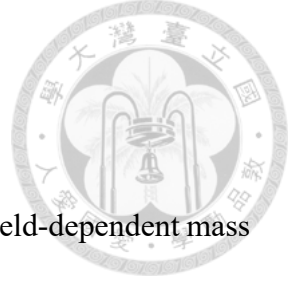
$$\Pi_B(T) = \left[\frac{1}{6} + \frac{N_g}{12} \left(\frac{11}{9} N_C + 3 \right) \right] g_1^2 T^2 \quad \underset{N_g=N_C=3}{=} \frac{11}{6} g_1^2 T^2, \quad (\text{D.16})$$

where N_g represents number of generations and N_C is a number of colors.

D.4 Top Quark

As only the top quark contribution is significant for our analyses, its field-dependent mass is

$$\overline{m}_t^2(\phi) = \frac{y_t^2}{2} \phi^2. \quad (\text{D.17})$$





Appendix E

An Illustrative Application PRM

Here we present an explicit example to demonstrate how the gauge dependence disappears in the PRM scheme. Consider a $SU_L(2) \times U(1)$ theory, the field is written as

$$H = \frac{1}{\sqrt{2}} \begin{pmatrix} \Phi_1 + i\Phi_2 \\ \Phi_3 + i\Phi_4 \end{pmatrix}. \quad (\text{E.1})$$

The generators* of those groups are

$$T^1 = \frac{1}{2} \begin{pmatrix} & & -1 \\ & 1 & \\ -1 & & \\ 1 & & \end{pmatrix}, \quad T^2 = \frac{1}{2} \begin{pmatrix} & & 1 \\ & & 1 \\ -1 & & \\ & -1 & \end{pmatrix},$$

$$T^3 = \frac{1}{2} \begin{pmatrix} & -1 & \\ 1 & & \\ & & 1 \\ & & -1 \end{pmatrix}, \quad T^4 = \frac{1}{2} \begin{pmatrix} & & & \\ -1 & & & \\ 1 & & & \\ & & -1 & \\ & & & 1 \end{pmatrix}.$$

*We use the real representation, *i.e.*, $-i$ is factored out. That is, $\mathbb{T} = -iT$, where T is what we adopt.

Note that $\{T^1, T^2, T^3\}$ are generators of isospin, and T^4 is for hypercharge. The Euclidean Lagrangian is

$$\mathcal{L}_E = \frac{1}{2}(D_\mu \Phi)_i^\dagger (D^\mu \Phi)_i + V_0(\Phi) + \frac{1}{4}W_{\mu\nu}^a W^{a\mu\nu}, \quad (\text{E.2})$$

$$\text{with } V_0(\Phi) = -\frac{1}{2}\mu^2\Phi^\dagger\Phi + \frac{1}{4}\lambda(\Phi^\dagger\Phi)^2, \quad (\text{E.3})$$



where Φ_i represents a vector $(\Phi_1, \Phi_2, \Phi_3, \Phi_4)$, $D_\mu \equiv \partial_\mu + g^a T^a W_\mu^a$, $W_\mu^a = \{W_\mu^1, W_\mu^2, W_\mu^3, B_\mu\}$ and $g^a = \{g_2, g_2, g_2, g_1\}$.

The field can be separated by the classical fields (ϕ_c) and quantum fields, $h(x)$:[†]

$$\Phi_i(x) = \phi_{c i} + \bar{h}_i(x), \quad (\text{E.4})$$

where $\phi_c = (0, 0, \phi, 0)$, and $\bar{h} = (h_1, h_2, h_3, h_4)$. The Higgs field is the third component of \bar{h} . The location of extrema of the Higgs potential at the tree level are

$$\phi_0^{(1)} = 0, \quad \phi_0^{(2)} = \pm\sqrt{\mu^2/\lambda} = \pm 246 \text{ GeV}. \quad (\text{E.5})$$

Let's expand Eq. (E.2) in terms of ϕ , arranging it in the power of the quantum field (h_i) and the gauge fields (W_μ). Then the Euclidean Lagrangian will be

$$\begin{aligned} \mathcal{L}_E = & \left(-\frac{1}{2}\mu^2\phi^2 + \frac{\lambda}{4}\phi^4 \right) + (-\mu^2\phi h_3 + \lambda\phi^3 h_3 + \partial_\mu h_i g^a T^a W_\mu^a \phi_{c i}) \\ & + \left[-\frac{1}{2}h_i \partial^2 h_i - \frac{1}{2}\mu^2 h_i^2 + \frac{\lambda}{4}(6\phi^2 h_3^2 + 2\phi^2 h_1^2 + 2\phi^2 h_2^2 + 2\phi^2 h_4^2) + \partial_\mu h_i g^a T^a W_\mu^a h_i \right] + \dots \\ & + \left[\frac{1}{2}W_\mu^a (\partial^2 g^{\mu\nu} - \partial^\mu \partial^\nu) \delta^{ab} W_\nu^b \right] + \left[(g^a T^a W_\mu^a \phi_c)^T (g^a T^a W_\mu^a \phi_c) \right] + \dots \end{aligned} \quad (\text{E.6})$$

Note that (1) since ϕ_c is independent of spacetime, its derivative is zero; (2) those terms with cubic and quadratic in ϕ_c and W_μ^a are omitted here; (3) the gauge field strength is

[†]This is called the background field method, a classical field are defined by: Euclidean action is minimized when the field value equals to the classical field. A quantum field is the field that fluctuates around the minimum.

cast by the following,

$$\begin{aligned}
& -\frac{1}{4}(\partial_\mu W_\nu^a - \partial_\nu W_\mu^a)(\partial^\mu W^{a\nu} - \partial^\nu W^{a\mu}), \quad gf^{abc}W_\mu^b W_\mu^c \text{ are omitted} \\
& = -\frac{1}{4}(\partial_\mu W_\nu^a \partial^\mu W^{a\nu} - \partial_\mu W_\nu^a \partial^\nu W^{a\mu} - \partial_\nu W_\mu^a \partial^\mu W^{a\nu} + \partial_\nu W_\mu^a \partial^\nu W^{a\mu}), \\
& = -\frac{1}{2}W_\nu^a(-\partial^2 W^{a\nu} + \partial_\mu \partial^\nu W^{a\mu}), \\
& = \frac{1}{2}W_\nu^a(\partial^2 g^{\mu\nu} - \partial^\nu \partial^\nu)\delta^{ab}W_\mu^b,
\end{aligned}$$

where we have integrated by parts and redefined μ and ν due to their symmetry. Eq. (E.6)

is equivalent to a more compact form:

$$\begin{aligned}
V_0(\phi_c) + \phi_i \frac{\partial V_0(\Phi)}{\partial \Phi_i} \Big|_{\phi_c} + \frac{1}{2}\phi_i \left(-\partial^2 + M_{ij}^2(\phi_c) \right) \phi_j + \partial^\mu \phi_i W_\mu^a (gT^a \phi_c)_i \\
+ \frac{1}{2}W_\mu^a \left((\partial^2 g^{\mu\nu} - \partial^\mu \partial^\nu)\delta^{ab} + m_A^2(\phi_c)^{ab} g^{\mu\nu} \right) W_\nu^b + \dots,
\end{aligned} \tag{E.7}$$

where

$$M_{ij}^2(\phi_c) = \frac{\partial^2 V}{\partial \phi_i \partial \phi_j} \Big|_{\phi_c}, \quad m_A^2(\phi_c)^{ab} = (g^b T^a(\phi_c)_i^T (g^a T^b(\phi_c)_i). \tag{E.8}$$

The explicit form of above can be understood by expanding the component in the potential:

$$\begin{aligned}
V_0(\Phi) & = -\frac{1}{2}\mu^2 \Phi_i \Phi_i + \frac{1}{4}\lambda(\Phi_i \Phi_i)^2, \\
& = -\frac{1}{2}\mu^2(h_1^2 + h_2^2 + (h_3 + \phi)^2 + h_4^2) + \frac{\lambda}{4}(h_1^2 + h_2^2 + (h_3 + \phi)^2 + h_4^2)^2,
\end{aligned} \tag{E.9}$$

and thus the derivative can be understood by the following: if $i \neq 3$,

$$\frac{\partial V_0}{\partial h_i} = -\mu^2 h_i + \frac{\lambda}{4}(4h_i h_j^2 + 4h_i^3 + 4h_i(h_3 + \phi)^2), \tag{E.10}$$

$$\frac{\partial^2 V_0}{\partial h_i \partial h_j} = -\mu^2 \delta_{ij} + \lambda \delta_{ij} (h_3 + \phi)^2 \tag{E.11}$$

$$+ \text{purely quantum field terms}, \tag{E.12}$$

$$\frac{\partial^2 V_0}{\partial h_i \partial h_j} \Big|_{h_c} = (-\mu^2 + \lambda \phi^2) \delta_{ij}, \tag{E.13}$$

and if $i = 3$,

$$\frac{\partial V_0}{\partial h_i} = -\mu^2(h_3 + \phi) + \lambda(h_3 + \phi)^3, \quad (\text{E.14})$$

$$\frac{\partial^2 V_0}{\partial h_i^2} = -\mu^2 + 3\lambda(h_3 + \phi)^2, \quad (\text{E.15})$$

$$\left. \frac{\partial^2 V_0}{\partial h_i^2} \right|_{h_c} = -\mu^2 + 3\lambda\phi^2. \quad (\text{E.16})$$



As a result, the scalar mass matrix, $M_{ij}^2(\phi_c)$, is

$$M_{ij}^2(\phi_c) = \begin{pmatrix} -\mu^2 + \lambda\phi^2 & & & \\ & -\mu^2 + \lambda\phi^2 & & \\ & & -\mu^2 + 3\lambda\phi^2 & \\ & & & -\mu^2 + \lambda\phi^2 \end{pmatrix}. \quad (\text{E.17})$$

The gauge bosons' mass matrix, $m_A^2(\phi)^{ab}$, is

$$\begin{aligned} m_A^2(\phi_c)^{ab} &= (g^b T^a(\phi_c)_i^T (g^a T^b(\phi_c)_i, \\ &= \begin{pmatrix} (g_2 T^1 \phi_c)^T g_2 T^1 \phi_c & (g_2 T^1 \phi_c)^T g_2 T^2 \phi_c & \dots \\ \vdots & (g_2 T^2 \phi_c)^T g_2 T^2 \phi_c & \dots \\ & & (g_2 T^3 \phi_c)^T g_2 T^3 \phi_c & (g_2 T^3 \phi_c)^T g_1 T^4 \phi_c \\ & & (g_1 T^4 \phi_c)^T g_2 T^3 \phi_c & (g_2 T^4 \phi_c)^T g_2 T^4 \phi_c \end{pmatrix}, \\ &= \frac{1}{4} \begin{pmatrix} g_2^2 & & & \\ & g_2^2 & & \\ & & g_2^2 & -g_2 g_1 \\ & & -g_2 g_1 & g_2^2 \end{pmatrix} \phi^2. \end{aligned} \quad (\text{E.18})$$

Notice that ab indices of the bracket represent the gauge fields' indices. The mixing term, $\partial^\mu \phi_i W_\mu^a (g T^a \phi_c)_i$, in Eq. (E.7) can be removed by imposing the gauge fixing condition,

$$\mathcal{F}^a = \partial^\mu W_\mu^a - \xi \phi_i (g T^a \phi_c)_i = 0, \quad (\text{E.19})$$

with the gauge fixing term

$$\begin{aligned}
\mathcal{L}_{\text{gf}} &= \frac{-(\mathcal{F}^a)^2}{2\xi}, \\
&= \frac{-1}{2\xi} [(\partial^\mu W_\mu^a)^2 - 2\xi \partial^\mu W_\mu^a \phi_i (gT^a \phi_c)_i + \xi \phi_i (gT^a \phi_c)_i \xi \phi_j (gT^a \phi_c)_j], \\
&= -\frac{(\partial^\mu W_\mu^a)^2}{2\xi} + \partial^\mu W_\mu^a \phi_i (gT^a \phi_c)_i - \frac{1}{2\xi} \xi \phi_i (gT^a \phi_c)_i \xi \phi_j (gT^a \phi_c)_j, \\
&= -\frac{(\partial^\mu W_\mu^a)^2}{2\xi} - W_\mu^a \partial^\mu \phi_i (gT^a \phi_c)_i - \frac{1}{2} \xi \phi_i m_A^2(\phi_c)_{ij} \phi_j,
\end{aligned} \tag{E.20}$$

where the last term is called gauge-fixing scalar boson mass matrix:

$$\begin{aligned}
m_A^2(\phi_c)_{ij} &= (gT^a \phi_c)_i^T \times (\phi_i (gT^a \phi_c)_j) \\
&= \begin{pmatrix} (g^a T^a \phi_c)_1^T (g^a T^a \phi_c)_1 & (g^a T^a \phi_c)_1^T (g^a T^a \phi_c)_2 & \dots & \\ \vdots & (g^a T^a \phi_c)_2^T (g^a T^a \phi_c)_2 & & \\ & & (g^a T^a \phi_c)_3^T (g^a T^a \phi_c)_3 & \\ & & & (g^a T^a \phi_c)_4^T (g^a T^a \phi_c)_4 \end{pmatrix}, \\
&= \frac{1}{4} \begin{pmatrix} g_2^2 & & & \\ & g_2^2 & & \\ & & 0 & \\ & & & g_2^2 + g_1^2 \end{pmatrix} \phi^2,
\end{aligned} \tag{E.21}$$

note that the ij indices of the bracket represent the scalar fields' indices. We also add in the ghost compensating terms:

$$\mathcal{L}_{\text{gh}} = \eta^{\dagger a} (-\partial^2 \delta^{ab} - \xi m_A^2(\phi_c)^{ab}) \eta^b + g f^{abc} (\partial^\mu \eta^{\dagger a}) - \xi (gT^a \phi_c)_i \eta^{\dagger a} \eta^b (gT^b \phi_c)_j.$$

$$\tag{E.22}$$

The full Lagrangian is then

$$\begin{aligned}
\mathcal{L}_E + \mathcal{L}_{\text{gf}} + \mathcal{L}_{\text{gh}} = & V_0(\phi_c) + \phi_i \frac{\partial V_0}{\partial \Phi_i} \Big|_{\phi_c} + \frac{1}{2} \phi_i \left(-\partial^2 + M_{ij}^2(\phi_c) - \xi m_A^2(\phi_c)_{ij} \right) \phi_j \\
& + \frac{1}{2} W_\mu^a \left\{ \left[\partial^2 g^{\mu\nu} - \left(1 - \frac{1}{\xi} \right) \partial^\mu \partial^\nu \right] \delta^{ab} + m_A^2(\phi_c)^{ab} g^{\mu\nu} \right\} W_\nu^b \\
& + \eta^{\dagger a} \left(-\partial^2 \delta^{ab} - \xi m_A^2(\phi_c)^{ab} \right) \eta^b + \dots,
\end{aligned} \tag{E.23}$$

where high order terms are omitted for simplicity. The results of loop-level potential calculation give us that

$$V_{\text{eff}}(\phi) = V_0(\phi) \tag{E.24}$$

$$- \frac{i}{2} \mu^{2\epsilon} \int \frac{d^d p}{(2\pi)^d} \left[\text{Tr} \ln(p^2 - M_{ij}^2 - \xi m_A^2(\phi)_{ij}) \right] \tag{E.25}$$

$$+ (d-1) \text{Tr} \ln(p^2 - m_A^2(\phi)^{ab}) + \text{Tr} \ln(p^2 - \xi m_A^2(\phi)^{ab}) \tag{E.26}$$

$$- 2 \text{Tr} \ln(p^2 - \xi m_A^2(\phi)^{ab}) + \dots \Big], \tag{E.27}$$

where \dots are field independent terms. A pre-factor, $d-1$, is from the dimension regularization (the conventional choice is $d = 4 - 2\epsilon$). This result shows that Eq. (E.25) comes from the scalar loop, Eq. (E.26) comes from the gauge loop; (E.27) is originated from the ghost loop. Note that the gauge dependence is cancelled out, if the scalar loop contribution is arranged into

$$\text{Tr} \ln(p^2 - M_{ij}^2 - \xi m_A^2(\phi)_{ij}) \longrightarrow \text{Tr} \ln(p^2 - M_{ij}^2) + \text{Tr} \ln(p^2 - \xi m_A^2(\phi)_{ij}); \tag{E.28}$$

As a consequence, the gauge dependence will be eliminated at the one-loop level. The main idea of the PRM scheme is to achieve the above arrangement. Let's first consider a matrix M whose matrix elements A, B , etc., are also matrices:

$$M = \begin{pmatrix} A & B \\ C & D \end{pmatrix}.$$

Since M can be arranged into

$$M = \begin{pmatrix} A & 0 \\ C & I \end{pmatrix} \begin{pmatrix} I & A^{-1}B \\ 0 & D - CA^{-1}B \end{pmatrix}, \quad (\text{E.29})$$



and the property of the determinant shows that $\det G = \det(TF) = \det(T) \det(F)$, its determinant is then

$$\det M = \det A \det(D - CA^{-1}B). \quad (\text{E.30})$$

If B, C are zeros, $\det M = \det A \det D$. As we know that $\ln \det M = \text{Tr} \ln M$,

$$\begin{aligned} \ln \det M &= \ln \det A + \ln \det D, \\ \text{Tr} \ln M &= \text{Tr} \ln A + \text{Tr} \ln D. \end{aligned} \quad (\text{E.31})$$

Back to our case, the matrix in Eq. (E.28) logarithm is

$$S_{ij} = p_{ij}^2 - M^2(\phi)_{ij} - \xi m_A^2(\phi)_{ij}. \quad (\text{E.32})$$

If S_{ij} is a block-diagonalized matrix which is crucial since in the most of the cases it is not; then M_{ab}^2 and m_{Acd}^2 are simultaneously diagonalizable but their eigenvalues live in distinct subspaces (*i.e.*, their eigenvalues are not mixed), then we have[‡]

$$\begin{pmatrix} p^2 I_{ab} - M_{ab}^2 & 0 \\ 0 & p_{cd}^2 - \xi m_{Acd}^2 \end{pmatrix}. \quad (\text{E.33})$$

As a result, combining Eq. (E.31), we finally have the separation:

$$\text{Tr} \ln S = \text{Tr} \ln(p^2 - M_{ab}^2) + \text{Tr} \ln(p^2 - \xi m_{Acd}^2). \quad (\text{E.34})$$

In this particular circumstance, we can eliminate the gauge dependence at the one-loop level. In the next section, we see how the gauge-invariant T_C can be got from the above formalism.

[‡]In the Sec. E.1, the upper left matrix is 1×1 , and the lower right matrix is 3×3

E.1 Gauge-invariant T_C



In this theory, similar to the condition in our model Eq. (2.38), the PRM scheme finds T_C when the condition,

$$V_0(\phi_0^{(1)}) + \hbar V_1(\phi_0^{(1)}, T_C, \xi) = V_0(\phi_0^{(2)}) + \hbar V_1(\phi_0^{(2)}, T_C, \xi), \quad (\text{E.35})$$

is satisfied; the minima are defined at Eq. (E.5). If ξ terms which mentioned in the previous section is cancelled, this particular T_C is gauge independent. In Eq. (E.35), the left hand side is gauge invariant which can be easily recognized: all the gauge dependent terms Eq. (E.18) and Eq. (E.21) in Eq. (E.25), Eq. (E.26) and Eq. (E.27) are all proportional to the classical background whose $\phi_0^{(1)} = 0$. The right hand side takes the EW-breaking minimum ($\phi_0^{(2)} = \sqrt{\mu^2/\lambda} = 246$ GeV). Therefore, the NG boson masses are equal to zero in this scheme, the scalar mass matrix Eq. (E.17) then becomes

$$M^2(\phi_0^{(2)})_{ij} = \text{diag}(0, 0, 2\mu^2, 0). \quad (\text{E.36})$$

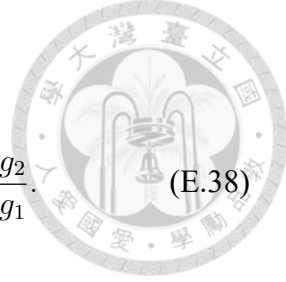
The gauge-fixing scalar boson mass matrix is then

$$m_A^2(\phi_0^{(2)})_{ij} = \frac{\mu^2}{4\lambda} \text{diag}(g_2^2, g_2^2, 0, g_1^2 + g_2^2). \quad (\text{E.37})$$

These two matrices actually can be arranged into the block-diagonalized form like Eq. (E.33), *i.e.*, $M^2(\phi_0^{(2)})_{ij}$ and $m_A^2(\phi_0^{(2)})_{ij}$ are simultaneously diagonalizable; their eigenvalues live in different subspace.[§] Therefore, the separation like Eq. (E.34) can be achieve. To see explicitly how $\text{Tr} \ln(p^2 - \xi m_A^2(h_0^{(2)})_{ij})$ eliminates $\text{Tr} \ln(p^2 - \xi m_A^2(h_0^{(2)})^{ab})$, we need to

[§]Note that this is not always valid, only when one evaluates the minima at the tree level.

diagonalize $m_A^2(\phi_c)^{ab}$, Eq. (E.18), through the rotation matrix

$$R^{ab} = \begin{pmatrix} 1 & & & \\ & 1 & & \\ & & \cos \theta_W & \sin \theta_W \\ & & -\sin \theta_W & \cos \theta_W \end{pmatrix}, \quad \tan \theta_W = \frac{g_2}{g_1}. \quad (\text{E.38})$$


After rotation, we have

$$R^{ab} m_A^2(\phi_c)^{bc} (R^T)^{cd} = \frac{1}{4} \begin{pmatrix} g_2^2 & & & \\ & g_2^2 & & \\ & & 0 & \\ & & & g_1^2 + g_2^2 \end{pmatrix} \phi^2. \quad (\text{E.39})$$

This is exactly the same as the gauge-fixing scalar boson mass matrix. Therefore, these two terms are cancelled out eventually. Finally, we show that T_C obtained from Eq. (E.35) is a gauge-independent result.



Bibliography

- [1] A. D. Sakharov, *Pisma Zh. Eksp. Teor. Fiz.* **5**, 32 (1967) [*JETP Lett.* **5**, 24 (1967)] [*Sov. Phys. Usp.* **34**, no. 5, 392 (1991)] [*Usp. Fiz. Nauk* **161**, no. 5, 61 (1991)].
- [2] A. D. Sakharov, *Sov. Phys. Usp.* **34**, no. 5, 417 (1991) [*Usp. Fiz. Nauk* **161**, no. 5, 110 (1991)].
- [3] N. S. Manton, *Phys. Rev. D* **28**, 2019 (1983); F. R. Klinkhamer and N. S. Manton, *Phys. Rev. D* **30**, 2212 (1984).
- [4] H. H. Patel and M. J. Ramsey-Musolf, *JHEP* **1107**, 029 (2011).
- [5] K. Fuyuto and E. Senaha, *Phys. Rev. D* **90**, no. 1, 015015 (2014).
- [6] S. Chatrchyan *et al.* [CMS Collaboration], *Phys. Lett. B* **716**, 30 (2012); G. Aad *et al.* [ATLAS Collaboration], *Phys. Lett. B* **716**, 1 (2012).
- [7] M. Laine and K. Rummukainen, *Nucl. Phys. Proc. Suppl.* **73**, 180 (1999)
- [8] C. P. Burgess, M. Pospelov and T. ter Veldhuis, *Nucl. Phys. B* **619**, 709 (2001); S. Profumo, L. Ubaldi and C. Wainwright, *Phys. Rev. D* **82**, 123514 (2010); Y. Mambrini, *Phys. Rev. D* **84**, 115017 (2011).
- [9] V. Silveira and A. Zee, *Phys. Lett.* **161B**, 136 (1985); J. McDonald, *Phys. Rev. D* **50**, 3637 (1994); C. P. Burgess, M. Pospelov and T. ter Veldhuis, *Nucl. Phys. B* **619**, 709 (2001); D. O'Connell, M. J. Ramsey-Musolf and M. B. Wise, *Phys. Rev. D* **75**, 037701 (2007); V. Barger, P. Langacker, M. McCaskey, M. J. Ramsey-Musolf and G. Shaughnessy, *Phys. Rev. D* **77**, 035005 (2008); S. Bhattacharya, P. Poulose and P.

Ghosh, JCAP **1704**, no. 04, 043 (2017); J. A. Casas, D. G. Cerdeo, J. M. Moreno and J. Quilis, JHEP **1705**, 036 (2017).



- [10] M. Garny and T. Konstandin, JHEP **1207**, 189 (2012).
- [11] C. L. Wainwright, S. Profumo and M. J. Ramsey-Musolf, Phys. Rev. D **86**, 083537 (2012).
- [12] S. P. Martin, Phys. Rev. D **90**, no. 1, 016013 (2014).
- [13] J. Elias-Miro, J. R. Espinosa and T. Konstandin, JHEP **1408**, 034 (2014).
- [14] D. Curtin, P. Meade and C. T. Yu, JHEP **1411**, 127 (2014).
- [15] N. K. Nielsen, Nucl. Phys. B **101**, 173 (1975).
- [16] R. Fukuda and T. Kugo, Phys. Rev. D **13**, 3469 (1976).
- [17] R. Jackiw, Phys. Rev. D **9**, 1686 (1974).
- [18] R. P. Feynman, Rev. Mod. Phys. **20**, 367 (1948).
- [19] S. Coleman and E. Weinberg, Phys. Rev. D **7**, 1888 (1973).
- [20] Koichi Funakubo, Shuichiro Tao and Fumihiko Toyoda, Prog. Theor. Phys. **114**, 2 (2005).
- [21] L. Dolan and R. Jackiw, Phys. Rev. D **9**, 3320 (1974).
- [22] D. Curtin, P. Meade and H. Ramani, arXiv:1612.00466 [hep-ph].
- [23] E. Braaten and R. D. Pisarski, Phys. Rev. Lett. **64**, 1338 (1990).
- [24] C. W. Chiang and E. Senaha, Phys. Lett. B **774**, 489 (2017).
- [25] C. W. Chiang, M. J. Ramsey-Musolf and E. Senaha, Phys. Rev. D, **97**, 015005 (2018).
- [26] Yann Mambrini, Phys. Rev. D **84**, 115017 (2011)
- [27] Carlos E Yaguna, JCAP, **2009**, 003 (2009)

- [28] M. Tanabashi *et al.* (Particle Data Group), Phys. Rev. D **98**, 030001 (2018).
- [29] T. Binder, T. Bringmann, M. Gustafsson and A. Hryczuk, arXiv: 1706.07433 [astro-ph.CO].
- [30] G. Belanger, F. Boudjema and A. Pukhov, arXiv:1402.0787 [hep-ph].
- [31] P. Athron, J. M. Cornell, F. Kahlhoefer, J. Mckay, P. Scott and S. Wild, arXiv:1806.11281 [hep-ph].
- [32] J. P. Ellis, Comput. Phys. Commun. **210**, 103 (2017).
- [33] M. D. Schwartz, Quantum Field Theory and the Standard Model. Cambridge University Press (2017).
- [34] L. Dolan and R. Jackiw, Phys. Rev. D **9**, 2904 (1974).
- [35] Andrew Fowlie, Comput. Phys. Commun. **228**, 264 (2018).

